Capillary Water Behavior During Evaporation of Granular Media

by

Shu Yang

Department of Mechanical Engineering and Materials Science
Duke University

Date:_______________________
Approved:

____
Tomasz A Hueckel, Supervisor

____
Josiah D. Knight

____
Piotr E Marszalek

Thesis submitted in partial fulfillment of
the requirements for the degree of
Master of Science in the Department of
Mechanical Engineering and Materials Science in the Graduate School
of Duke University

2018

ABSTRACT

by

Shu Yang

Department of Mechanical Engineering and Materials Science
Duke University

Date:_______________________
Approved:

____
Tomasz A Hueckel, Supervisor

____
Josiah D. Knight

____
Piotr E Marszalek

An abstract of a thesis submitted in partial
fulfillment of the requirements for the degree
of Master of Science in the Department of
Mechanical Engineering and Materials Science in the Graduate School of
Duke University

2018

Abstract

Intense studies on evaporation in fluid systems have been conducted over the past decades, mainly on sessile droplets which are the simplest bodies to simulate. In this thesis, the evaporation process of a water bridge between two spherical grains is studied. A multi-physics approach is adopted focusing on the evaporation dynamics, the flow motion in liquid, the pressure distribution inside the water bridge, and the vapor behavior combined with the movement of free interface.

Dedication

To my grandfather, who encourage to pursue higher degree of education but passed away one week before I was enrolled by Duke University.

Contents

List of Figures

Acknowledgements

I sincerely thank my advisor, Dr. Tomasz Hueckel for his guidance and encouragement to make this project possible. His wide knowledge and enthusiasm have always been a source of inspiration. His spirit at devote onto science has changed my perspective on the research.

The experimental data have been obtained at the University of Montpellier, Montpellier, France by Dr. B. Mielniczuk, Professors S.M. Youssoufi and Tomasz Hueckel. I greatly appreciate the possibility of using these data before their publication.

I am grateful to Bangxin Lan who has taught me to build the geometry model and obtain asymptotic function. His professional advice plays an important role in this research.

I am grateful to all of people who supported me in any aspect at Duke University.

1. Introduction

1.1 Subject of the research

The capillarity phenomena are encountered in various areas of mechanical engineering, chemical engineering, and geo-engineering. They are encountered in people's everyday life, such as rain drop and a floating ant. Most of them are too familiar to be given a special notice. The first observation of capillary rise phenomenon can be traced back to the Middle Ages. This phenomenon could not be explained until the experiments by Leonardo da Vinci, who has later termed it as capillary which means hair-like in Latin, for the hair-size internal diameter of the vessels in which the phenomenon is observed.

It has become clear that several phenomena arise when two fluids are adjacent and immiscible to each other. They become separated by capillary surface that is used to conceptualize the free interface called also meniscus from greek (moon-like) that forms at equilibrium between two kinds of immiscible fluid, such as water and gas.

This study focuses on a mechanism of coupling in liquids between chemical processes (diffusion and mass phase transition), and mechanical properties and processes (pressure distribution and flow field). In particular, the evaporation process of water bridge between two spherical grains is addressed in. This mechanism is of vital importance in soil mechanics. Soil in general consists of particles water and gas and in configurations after leading to forming capillary water bridge. The water bridge between two grains is the most basic model because larger and more complex bridges will eventually break up to this configuration due to advanced evaporation.

Besides experiments and theoretical analyses, numerical simulations of free interface are an important method of study of evaporation. The simulation methods have been developing over decades and substantial progress was made in the research of capillarity. This study focuses on the numerical simulations of evaporation process of a water bridge between two grains. A better understanding of how pressure distribution and flow field change as the result of evaporation is believed to be essential for many applications in hydrology, printing technologies, petroleum engineering, etc.

1.2 Motivation

The behavior of sessile droplet on the substrate has been studied for hundreds of years. The most prominent theory of surface tension effects was proposed by Thomas Young and Pierre-Simon Laplace (1805-1806). This theory states that pressure difference between gas and liquid across the interface is proportional to the mean surface curvature. The Young-Laplace theory implies also that contact angle is a constant, which is not supported by experiments. Although the droplet is the simplest geometry for which capillary force plays an important role, the Young-Laplace theory is complex enough to predict the real situations of drying of sessile droplet by coupling the pressure and the interface curvature of contour in the presence of evaporation. However, a comprehensive analysis of the behavior of evaporating bodies of a more complex geometry, such as capillary bridges, is still lacking.

Capillary phenomena play an important role in real life and technology. The capillary effect appears in a thin tube, between the hair of a brush, in porous material, such as paper or in a cell. During ink printing, the liquid bridges forms at the contact between the ink and paper. The flow may develop within the ink body and the paper can be deformed as a result. The quality of the print can be hence negatively influenced. The current study can be helpful to improve the technology of the ink printing.

There has been a growing understanding of the relationship between evaporation flux and flow field in sessile droplet. Deegan [1] postulated that the evaporation flux induces a flow field inside a droplet. Similarly, the evaporation process will hence induce various changes of water bridge, including its geometric shape, the interface position, and the pressure distribution inside the water bridge. It is conceivable that the flow field can be produced inside the evaporating liquid. Knowing the mechanism of the process would be helpful to describe a number of phenomena, among others such as the strength difference of dry soil and wet soil and the sedimentation of particles.

However, no analytical solution is known to precisely describe the phenomena inside the water bridge during evaporation with the moving interface. Hua Hu [2] and his coworkers simulated the evaporation of a water sessile drop on glass substrate in air. Brutin and Starov [3] made a review of advanced simulation of sessile drop during evaporation. Many simulations of sessile droplet during evaporation were produced in past several years. The researchers explained such phenomenon, such as flow field inside the droplet, are related to capillarity and evaporation flux [2]. The capillarity and evaporation flux play an important role in the evaporation process of water bridge. Numerical simulations of evaporation of water bridge can help to explain the internal flow phenomenon and test the previous conclusion.

1.3 Background

1.3.1 Concept of capillary water bridge

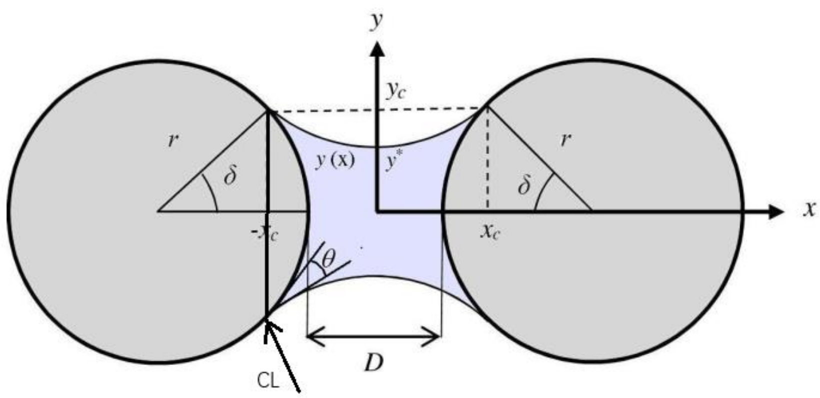

Figure 1: Contact line and Contact angle [4]

Liquids tend to form bridges between the proximity points of their solid surfaces. The formation is due to adhesive force arising between liquid and solid mainly caused by the presents of surface tension at the interface between liquid and gas. Surface tension makes the interface curved to maintain the equilibrium. If the mean curvature is negative, the pressure difference across the interface is proportional to the mean of the two normal curvatures of the interface, as stated by Young-Laplace laws.

$$p_a - p_l = \sigma_{lg}(\frac{1}{r_g} + \frac{1}{r_{ext}}) \tag{1}$$

where σ_{lg} is the liquid surface tension, r_g and r_{ext} are radius of curvature of the bridge at its gorge and at its side, respectively. This induces a negative pressure in the liquid.

The contact angle and contact line are important in studying the evaporation process. Contact angle (CA) refers to the angle θ between the tangent line of gas-liquid phase and tangent line of solid-liquid phase at the intersection of gas, liquid, and solid phase. Contact line (CL) refers to the intersecting line of gas, liquid, and solid phase.

At equilibrium the bridge must be such that at the contact line of the phases the contact angle is expressed through:

$$\cos\theta_e = \frac{\sigma_{sg} - \sigma_{sl}}{\sigma_{lg}} \tag{2}$$

where θ_e is the contact angle at equilibrium; σ_{sg} is surface tension of solid-gas interface; σ_{sl} is surface tension of solid-liquid interface; σ_{lg} is surface tension of liquid-gas interface

If the three forces are balanced on the three-phase contact line, the water bridge is stationary. σ_{sg}, σ_{sl}, and σ_{lg} are the physical properties of liquid, gas and solid. Their value should be constant for a specific situation. Therefore, θ_e should be a constant contact angle during evaporation if it is slow. However, the experiments find the contact angle that makes the water bridge be stationary during evaporation and also extension varies within a range of values. As a result, the contact line pins and the contact angle decreases and the bridge changes its form. This phenomenon is called pinning. When the contact angle decreases to a critical value, the contact line recedes while the contact angle becomes constant. This phenomenon is called depinning [2].

1.3.2 Summary of relative past research

Mielniczuk et al [4] present a number of analogies between the behavior during evaporation of water bridge and sessile drop. The hysteresis of contact angle and the pinning and depinning of contact line of water bridge are observed in both cases. The water bridge contact line pins at first, while when the contact angle decreases to a minimum receding angle θ_r depinning occurs. The phenomenon is interesting and important from physics point of view, while the causes of it remain elusive. The process of evaporation includes the phase transition at the free interface the vapor transfer in the environment, the evolution of the free interface and the flow inside the liquid bridge.

The Young-Laplace equation is used to determine the capillary pressure of the water bridge at the interface by measuring a set of variables of the geometric shape of the water bridge [3,4]. The volume of water bridge and the two principal surface curvatures at the bridge gorge, and the external curvature at the neck of the bridge, should be measured to determine the capillary pressure. Numerous researchers make efforts to describe analytically the surface shape of the bridge by using Laplace-Young equation without considering evaporation. Gagneux and Millet [5] classified the water bridges free surface as either a nodoid, catenoid or unduloid and described their shape via differential equations. However, these equations are too complicated to determine the static geometric shape of water bridge analytically.

The "coffee ring" is another phenomenon during the evaporation of sessile droplet. Similar phenomenon appears in water bridge. Figure 2 shows the phenomenon that the residue left to generate a dark and concentrated ring along the perimeter of stain during the drying of a droplet of coffee. Deegan and his coworkers [6] proposed that an outward flow was generated when the contact line was pinned. Such flow could remove all the solute to the contact line. Deegan also successfully predicted the relationship between the mass of residue and time. In what follows any solute is ignored in the liquid phase.

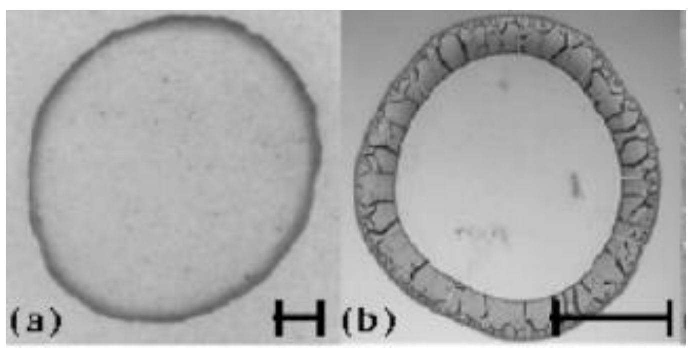

Figure 2: (a)Coffee stain; (b) dried colloidal microsphere [6]

Murisic [7] classified the evaporation models into three types: models which consider all transfer phenomena in liquid and gas phase; models which simplified the process of transport as diffusion; and finally models, which are applicable to strongly volatile liquid, where Marangoni effects become important due to thermal instability.

Most of the research focuses on weakly volatile liquids, such as water, that evaporates into static air. The purely diffusive approach is followed also in this work.

Based on the analogy of water bridge and sessile drop behavior, two assumptions are made. The process of evaporation is regarded as a steady state process. It is hence assumed that the time variable can be omitted in the diffusion equation of vapor, as the concentration of vapor is established at a smaller time scale than the time scale of the whole evaporation process.

Capillary force refers to the interparticle force between a series of unsaturated granular particles. It is generated by two effects: pore water pressure in the capillary bridge and surface tension at the contact. The capillary force produces a tendency to pull granular particles together. Therefore, it is believed that the capillary adhesion forces bring an apparent increase of strength to moist granular materials, such as soil [8].

To clarify the mechanisms of the adhesion, Mielniczuk et al [2] studied the evaporation of 4μl capillary water bridge between two grains in the static air. The experiments focus on obtaining the relationship among mass loss of liquid, time, distance of separation of two 8mm grains, capillary force, and volume of liquid. The mass of water was observed to linearly decrease with time between 0 and 30 mins. The change of capillary force with volume loss was obtained from the experiments. The capillary force changes non-monotonously with the relative loss of water. It first increases from the relative volume loss of 0 to 0.5, and it decreases from the relative volume loss of 0.5 to 1. Based on the measured normal curvatures of the interface, capillary pressure has been calculated for 4 points of the variables profile, for 3 different grain separations, of 1.3mm, 0.7mm and 0.3mm, using Laplace equation (1). The pressure appears to evolve substantially as showed in the Appendix for separation of 1.3mm. These experimental results are the basis for comparison of the numerical results obtained.

1.3.3 Numerical simulation of evaporation

Great majority of numerical simulations of liquid evaporation focus on the sessile drop. The main difficulty to simulate the evaporation process of water bridge results from its variable geometric shape. To reduce the troubles with the location of free interface, many simulations are conducted assuming either a constant contact angle or a fixed contact line. In reality both are variable during evaporation. Alternative simulations couple the evolution of free interface with the calculations of the evaporation flux to obtain the volume variation of the liquid with time. For instance, Hua Hu and his coworkers [9] simulated the evaporation of water sessile drop on glass substrate in air. Under the assumption that the temperature is constant, they obtained the local evaporation flux in each time step and integrated it over the area of interface and time to deduce the contour of liquid. The evolution of the free interface with time was then obtained. The moving interface problem was transferred to a series of fixed interface problems. The simulation of water bridge between two grains under similar assumptions is yet to be performed.

1.4 Theoretical basis of numerical simulation of evaporation of water bridge

Besides experiments and theoretical analysis, numerical simulations of free interface are another important method of studying the of evaporation of capillary bridges. There are several advantages of numerical simulation:

a. The liquid flow during the evaporation of the water bridge is complicated, hence existing analytical solutions are hard to obtain, while the validity range of the solution is limited. Finally, numerical simulation can provide the solutions that are better suited for parametric studies.

b. Compared to an experiment, a numerical simulation can overcome limitations of the measurements and provide assessment of the variables, such as the distribution of evaporation flux and flow field inside the liquid. By providing such assessment, simulations can decrease the cost and time of the experiments.

1.4.1 Lagrange and Euler description of fluid flow within capillary bridges

Because of significant displacements of the interface and its interplay with discretization grids the systems of reference for variables have a crucial role. The numerical simulations are based on the conservation law of mass, the conservation law of momentum, and the conservation law of energy. Lagrange and Euler proposed two classical methods of description of velocity, which gave rise to now classical Lagrange and Euler descriptions of all variables involved.

Accordingly, the method in which a differential equation is expressed in the coordinate system that is established on a moving particle is called Lagrange description. An alternative method in which the differential equation is formulated in the coordinate system that is fixed in space is called Euler description. According to the adopted descriptions, the types of mesh of finite element method are different and the resulting differential equations are different. Compared to the Lagrange description, Euler description is more frequently used in fluid mechanics, because the movement of material particles varies acutely in flow problems. However, the complicated variation of relative position of the particles will generate the distortion of the mesh, possibly generating a meshing singularity which impedes further calculation. On the other hand, Lagrange description possesses an important advantage that the nodes of mesh always coincide with particles, which makes it easier to obtain the solution of control equations. It is also more precise to locate the free interface.

Locating the position of the free interface is a pivotal problem in dealing with the evaporation problem of water bridge. The precision of location of the free interface affects the calculation of surface tension, and further influences the shape of water bridge, flow velocity and other aspects. There are two methods in locating the position of free interface: Interface Tracking and Interface Capturing. Although Lagrange description can accurately track the free interface, it is much more complicated than Euler description in realizing the numerical value. The computational domain should be meshed after under each time step which results in long periods to obtain the results.

Although Euler description is valid in analyzing the whole flow field, the fact that the mesh is fixed in space leads to the disadvantage that the free interface cannot be precisely located. To alleviate the problem, an interface tracking should be introduced. Volume of fluid (VOF) is the most frequently used method. It is based on a function of volume of fluid whose definition is a ratio of volume of target fluid to the volume of a mesh cell. Figure 3 shows the idea of volume of fluid. In a grid around free interface, there are liquid phase and gas phase at the same time. There are cells where only liquid phase in the mesh of liquid, so that the VOF function for the cell has a value of 1. If there is only gas phase in the mesh cell, so that the function value is 0. If the value of VOF function in each cell is obtained, the location of the interface can be tracked.

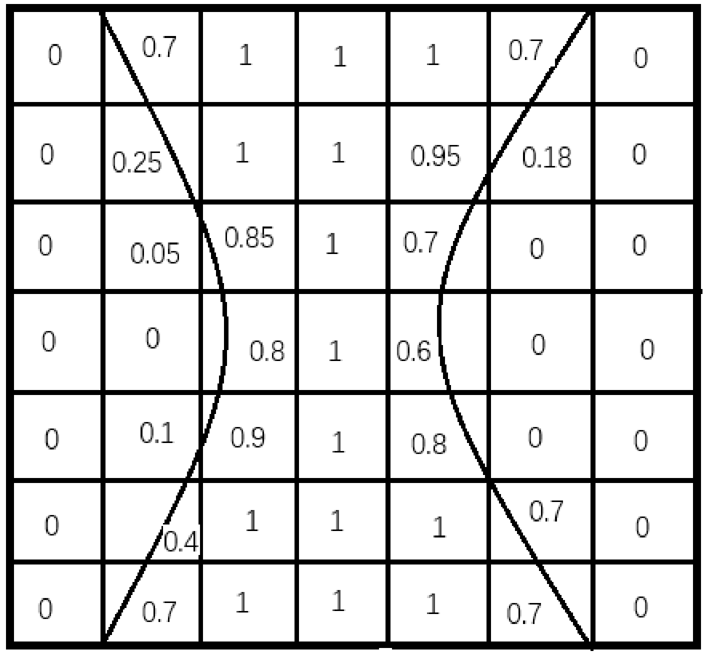

Figure 3: Schematic of volume of fluid method

An alternative method is level-set method. The basic idea is that the free interface is regarded as the zero-level set of a function φ in a higher dimension space (Figure 4). The velocity of free interface is also applied in higher dimensional level-set function. The evolution equation that satisfies the level-set function is solved. Then the level-set function is advanced. Finally, the zero-level set of level-set function is calculated at a new time. The shape of free interface can be obtained

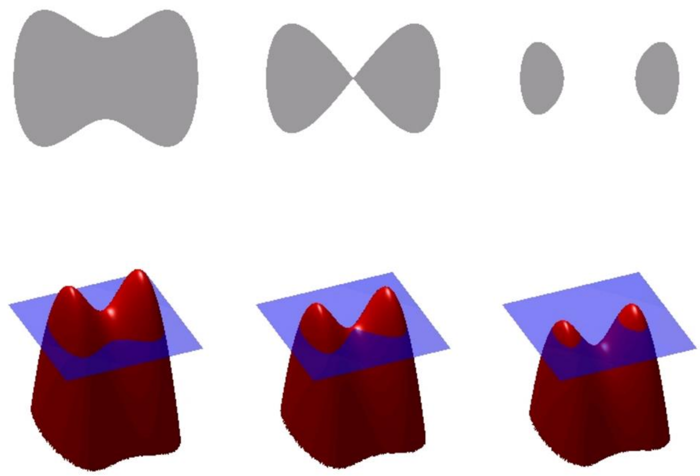

Figure 4: Schematic of level-set method [10]

Although the volume of fluid and level-set method compensate the deficiency of Euler description in some degree, they still have obvious defects. For the volume of fluid, the discontinuity (0 or 1) of volume fraction limits the accuracy of calculation of the position of free interface and the mean curvature which will affect the simulation of Laplace pressure. In contrast, the level-set method possesses higher accuracy in determining the position of free interface. However, the advance of the level-set function is not conservative. The distortion of the flow field can be highlighted during the calculation.

1.4.2 The Arbitrary Lagrange-Euler (ALE) method

Considering the advantages and disadvantages of Lagrange description and Euler description, a new method (ALE) which combines their advantages has been proposed. Noh [11] described the basic idea of ALE in 1963. Donea [12] and Belytschko

[13] followed the idea and applied ALE to finite element method in the research of the transient coupling problem of liquid and solid.

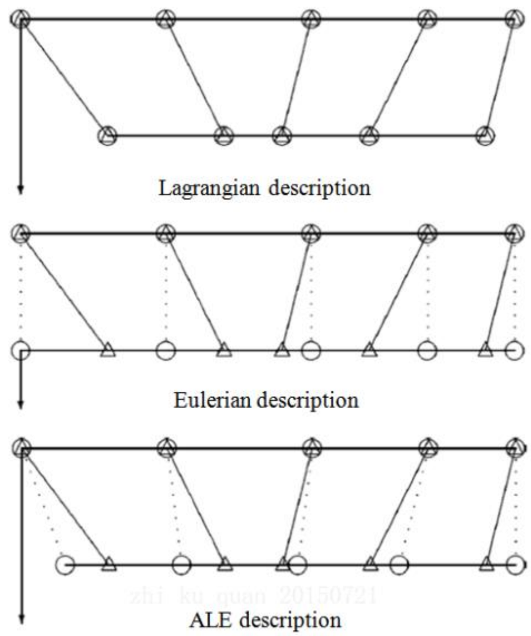

Figure 5: One-dimensional example of Lagrangian, Eulerian and ALE mesh and particle motion. [10]

Figure 5 shows the main idea of ALE. In addition to the previously mentioned, an additional coordinate system is introduced that is the coordinate system of the mesh. The movement of the mesh coordinate system is independent of the space coordinate system and the material coordinate system. It can either follow the movement of material which is Lagrange description on the free interface or coincide with space coordinate system in the internal fluid which is Euler description. This characteristic makes the calculation adapt the shape of calculation domain by adjusting the mesh in calculation domain. The distortion of mesh is alleviated.

1.4.3 The basic equations of Arbitrary Lagrange-Euler (ALE) method [10]

The transport equation can be deduced in two-dimensional Cartesian coordinate system. $\boldsymbol{\Omega}_{x}$ denotes the space coordinate of Euler description. $\boldsymbol{\Omega}_{X}$ denotes the material coordinate of Lagrange description. $\boldsymbol{\Omega}_{Xm}$ denotes the mesh coordinate system. $\boldsymbol{X}$ and $\boldsymbol{X}_m$ denote the material coordinate of material point and mesh coordinate of mesh point, respectively. $\boldsymbol{x}(\boldsymbol{X}, t)$ and $\boldsymbol{x}_m(\boldsymbol{X}_m, t)$ denote the space coordinate of material point and space coordinate of mesh point at time t.

The velocity of material can be deduced:

$$\boldsymbol{u}(\boldsymbol{X}, t) = \frac{\partial \boldsymbol{x}(\boldsymbol{X},t)}{\partial t} \tag{3}$$

The velocity of mesh can be deduced:

$$\boldsymbol{u}(\boldsymbol{X}_m, t) = \frac{\partial \boldsymbol{x}_m(\boldsymbol{X}_m,t)}{\partial t} \tag{4}$$

The same function f can be described as $f(\boldsymbol{X}, t)$, $f(\boldsymbol{x}, t)$, and $f(\boldsymbol{X}_m, t)$ in Lagrange coordinate system, Euler coordinate system and ALE coordinate system.

$$\frac{Df}{Dt} = \begin{cases} \frac{\partial f(\boldsymbol{X},t)}{\partial t} + \frac{\partial f(\boldsymbol{X},t)}{\partial \boldsymbol{X}} \frac{\partial \boldsymbol{X}}{\partial t} & Lagrange \\ \frac{\partial f(\boldsymbol{x},t)}{\partial t} + \frac{\partial f(\boldsymbol{x},t)}{\partial \boldsymbol{x}} \frac{\partial \boldsymbol{x}}{\partial t} & Euler \\ \frac{\partial f(\boldsymbol{X}_m,t)}{\partial t} + \frac{\partial f(\boldsymbol{X}_m,t)}{\partial \boldsymbol{X}_m} \frac{\partial \boldsymbol{X}_m}{\partial t} & ALE \end{cases} \tag{5}$$

Material point is fixed in the material coordinate system. Therefore, in Lagrange description:

$$\frac{\partial \boldsymbol{X}}{\partial t} = 0 \tag{6}$$

$$\frac{Df}{Dt} = \frac{\partial f(\boldsymbol{X},t)}{\partial t} \tag{7}$$

In Euler description,

$$\frac{\partial f(\boldsymbol{x},t)}{\partial t} + \frac{\partial f(\boldsymbol{x},t)}{\partial \boldsymbol{x}}\frac{\partial \boldsymbol{x}}{\partial t} = \frac{\partial f(\boldsymbol{x},t)}{\partial t} + \frac{\partial f(\boldsymbol{x},t)}{\partial \boldsymbol{x}} \cdot \boldsymbol{u}(\boldsymbol{X},t) \tag{8}$$

In ALE description with applying the chain rule,

$$\frac{\partial f(\boldsymbol{X}_m,t)}{\partial \boldsymbol{X}_m}\frac{\partial \boldsymbol{X}_m}{\partial t} = \frac{\partial f(\boldsymbol{X}_m,t)}{\partial \boldsymbol{x}}\frac{\partial \boldsymbol{x}(\boldsymbol{X}_m,t)}{\partial \boldsymbol{X}_m}\frac{\partial \boldsymbol{X}_m}{\partial t} \tag{9}$$

If function f is substituted by coordinate $\boldsymbol{x}$, then its derivative becomes

$$\frac{D\boldsymbol{x}}{Dt} = \begin{cases} \frac{\partial\, x(\boldsymbol{X},t)}{\partial t} = \boldsymbol{u}(\boldsymbol{X},t) & Lagrange \\ \frac{\partial\, x(\boldsymbol{X}_m,t)}{\partial t} + \frac{\partial\, x(\boldsymbol{X}_m,t)}{\partial \boldsymbol{X}_m}\frac{\partial \boldsymbol{X}_m}{\partial t} = \boldsymbol{u}(\boldsymbol{X}_m,t) + \frac{\partial\, x(\boldsymbol{X}_m,t)}{\partial \boldsymbol{X}_m}\frac{\partial \boldsymbol{X}_m}{\partial t} & ALE \end{cases} \tag{10}$$

The second term of the LHS of equation (10b) can be re-written as

$$\frac{\partial\, x(\boldsymbol{X}_m,t)}{\partial \boldsymbol{X}_m}\frac{\partial \boldsymbol{X}_m}{\partial t} = \boldsymbol{u}(\boldsymbol{X},t) - \boldsymbol{u}(\boldsymbol{X}_m,t) \tag{11}$$

If the RHS of equation (11) is defined as convection velocity as $\boldsymbol{u}_c$,

$$\boldsymbol{u}_c = \boldsymbol{u}(\boldsymbol{X},t) - \boldsymbol{u}(\boldsymbol{X}_m,t) \tag{12}$$

then equation (5), by substituting equation (9), (11), and (12), becomes

$$\frac{Df}{Dt} = \frac{\partial f}{\partial t} + (\boldsymbol{u}_c \cdot \nabla)f \tag{13}$$

where ∇ is spatial gradient operator.

If $\boldsymbol{u}(\boldsymbol{X}_m,t) = 0$, $\boldsymbol{u}_c = \boldsymbol{u}(\boldsymbol{X},t)$. The mesh is fixed in space coordinate system. The ALE description becomes to Euler description. If $\boldsymbol{u}_c = 0$, the mesh is fixed in material coordinate system. The ALE description becomes to Lagrange description.

The Navier-Stokes equation of incompressible fluid is

$$\rho\frac{d\boldsymbol{u}}{dt} = \nabla \cdot [-p\boldsymbol{I} + \mu(\nabla\boldsymbol{u} + (\nabla\boldsymbol{u})^T)] \tag{14}$$

In Euler description

$$\frac{d\boldsymbol{u}}{dt} = \frac{\partial \boldsymbol{u}}{\partial t} + (\boldsymbol{u} \cdot \nabla)\boldsymbol{u} \tag{15}$$

Therefore, the Navier-Stokes equation of incompressible fluid in Euler description becomes

$$\rho\left(\frac{\partial \boldsymbol{u}}{\partial t} + (\boldsymbol{u} \cdot \nabla)\boldsymbol{u}\right) = \nabla \cdot [-p\boldsymbol{I} + \mu(\nabla\boldsymbol{u} + (\nabla\boldsymbol{u})^T)] \tag{16}$$

In ALE description

$$\frac{d\boldsymbol{u}}{dt} = \frac{\partial \boldsymbol{u}}{\partial t} + (\boldsymbol{u}_c \cdot \nabla)\boldsymbol{u} \tag{17}$$

Therefore, the Navier-Stokes equation of incompressible fluid in ALE description becomes

$$\rho\left(\frac{\partial \boldsymbol{u}}{\partial t} + (\boldsymbol{u}_c \cdot \nabla)\boldsymbol{u}\right) = \nabla \cdot [-p\boldsymbol{I} + \mu(\nabla\boldsymbol{u} + (\nabla\boldsymbol{u})^T)] \tag{18}$$

The ALE description introduces a new variable $\boldsymbol{u_c}$ which increase a degree of freedom. New restricted condition of the velocity needs to be introduced. A new efficient algorithm of movement of mesh is necessary. The movement of mesh can be controlled by controlling the velocity of material $\boldsymbol{w}(\boldsymbol{X}, t)$

$$\boldsymbol{w}(\boldsymbol{X}, t) = \frac{\partial \boldsymbol{X}_m(\boldsymbol{X}, t)}{\partial t} \tag{19}$$

According to equation (11)

$$\boldsymbol{u}_c = \boldsymbol{u}(\boldsymbol{X}, t) - \frac{\partial\, \boldsymbol{x}(\boldsymbol{X}_m, t)}{\partial \boldsymbol{X}_m}\boldsymbol{w}(\boldsymbol{X}, t) \tag{20}$$

In conclusion, the convection velocity $\boldsymbol{u}_c$ is consisted in the introduction of a new, fictitious variable, the solution for fluid allows to calculate the actual velocity $\boldsymbol{u}(\boldsymbol{X}, t)$.

2. Objectives and tasks

The objective of this capillary study is to formulate a better understanding of the evaporation process of water bridge between two grains. The particular interest is the evolution of the distribution of Laplace pressure within the water bridge, as well as the flow of liquid within the water bridge. The processes should be simulated and compared to the experimental data.

Specific tasks to be undertaken include:

- To establish the effects of vapor concentration in the process zone with diffusion.
- To establish quantitative relationships between vapor transport and flow field.
- To track the position of liquid-gas interface.
- To simulate the flow field inside the water bridge.
- To simulate the vapor flow in gas phase.
- To simulate the pressure distribution at the interface of the water bridge.
- To analyze the simulation results in the light of the experimental results.
- To outline possible further improvements of models.

3. Numerical simulation of evaporation of water capillary bridge

3.1 Introduction to COMSOL

COMSOL commercial code has been adopted for the simulation. COMSOL Multiphysics is focused on multi-physics couplings mainly in liquids. COMSOL simulates the real physical phenomena by solving partial differential equations (PDEs) based on finite element method (FEM). The main characteristics COMSOL are the open architecture, and the properties of materials and the boundary conditions that are controlled by parameters, powerful meshing and computation. Users can not only apply the professional model library, but can also enter their own partial differential equations to simulate the physical phenomena in COMSOL Multiphysics.

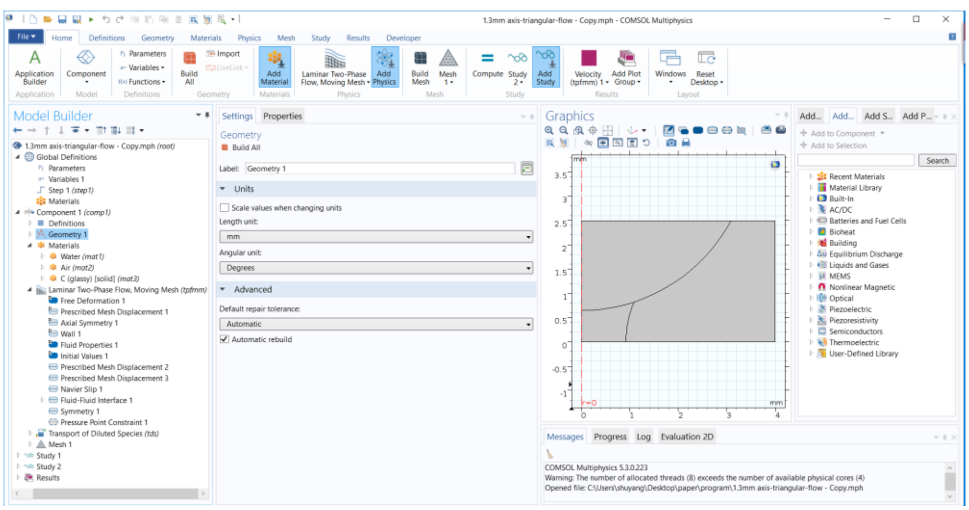

Figure 6: Interface of COMSOL

The evaporation process of water bridge considered in this paper, includes two glass balls which constitute solid phases, water bridge which is liquid phase, and infinite air condition which is gas phase. The following COMSOL modules were employed for simulation: Laminar Two-phase Flow, Moving Mesh and Transport of Diluted Species. Laminar Two-phase Flow, Moving Mesh can be used to calculate the two-phase flow of two immiscible fluids which are separated by a moving interface. The position of interface can be precisely calculated by transforming the grids. The meaning of moving mesh is that the grids can move along the boundary of material. The flow in liquid phase and gas phase can by calculated by this module. Transport of Diluted Species can be employed to calculate the transport of diluted species in the mixtures, solution, and solid. It is used to calculate the diffusion of vapor in the air.

3.2 Basic assumption of model

The evaporation process of water bridge is complicated. It includes the two-phase flow, the evolution of interface, and the dispose of the motion of contact line. There are five assumptions of the simulation:

(1) The scale of geometrical model is small enough. The radius of contact line is less than 1.3mm which makes Bo<<1. The influence of gravity is weak compare to surface tension. Therefore, the gravity is neglected [14].

(2) For simplicity, the geometrical shape of the water bridge is modeled by COMSOL Geometry which is closed to the contour of experimental results [15]. Once the

evaporation occurs, the interface shape will change under various boundary conditions. The position of interface is a result of solution of the problem.

(3) The time scale of the penetration of molecules through the interface, which is about 10^{-10}s, is much less than the time scale of diffusion ($t_{scale}=R_c^2/D\sim10^{-2}$s) [16]. Hence, it is assumed that evaporation process is limited by the transport of vapor. Therefore, a model is employed which couples the transport process of vapor in gas phase with the liquid phase by boundary condition of concentration. The vapor near the interface is regarded as saturated.

(4) Lee K [17] and coworkers stated that the convection in the static air did not obviously affect the evaporation process. Therefore, convection is not considered.

(5) The flow velocity of liquid is slow enough (Ma<<0.3), which means that the gas and liquid can be regarded as incompressible fluid. The variation range of pressure and temperature is not obvious, the surface tension and other physical parameters are regarded as constants.

3.3 Governing equations of model

Based on the above assumptions, there are three governing equations:

(1) The Navier-Stoke equation in liquid phase and gas phase of incompressible fluid

$$\rho\left(\frac{\partial \boldsymbol{u}}{\partial t}+(\boldsymbol{u_c}\cdot\nabla)\boldsymbol{u}\right)=\nabla\cdot\left[-p\boldsymbol{I}+\mu(\nabla\boldsymbol{u}+(\nabla\boldsymbol{u})^T)\right]+\boldsymbol{F} \tag{20}$$

where ρ is the density of fluid, $\boldsymbol{u}$ is the fluid velocity, t is time, $\boldsymbol{I}$ is identity matrix, μ is dynamic viscosity, and $\boldsymbol{F}$ is the volume force. Because the gravity is neglected, $\boldsymbol{F}$ will be ignored in the equation.

(2) The equation of continuity in liquid and gas phase:

$$\nabla \cdot \boldsymbol{u} = 0 \tag{21}$$

(3) The diffusion equation of vapor in gas phase:

$$\frac{\partial c}{\partial t} = \nabla \cdot (D \nabla c) \tag{22}$$

Where c is concentration of vapor, and D is diffusion coefficient.

3.4 Boundary conditions

Boundary conditions need to be specified for Laminar Two-phase Flow, Moving Mesh and Transport of Diluted Species sub-routines.

3.4.1 Boundary conditions of Laminar Two-phase Flow, Moving Mesh

The Laminar Two-phase Flow, Moving Mesh Modules are based on ALE description. As derived earlier, the ALE description introduces the freedom of mesh which requires the specification. In what follows, the boundary conditions for this module include the physical boundary conditions and mesh boundary conditions.

(1) Physical boundary conditions

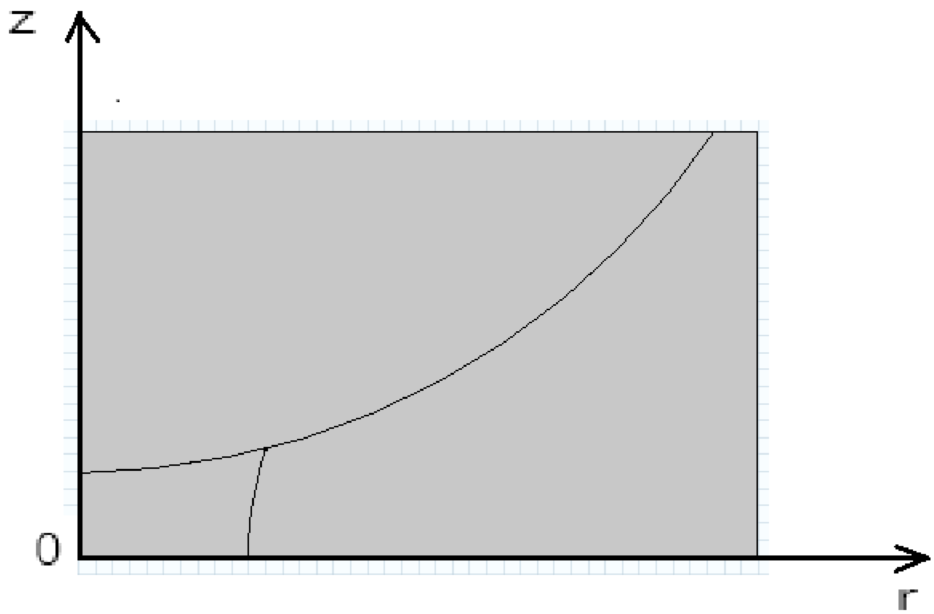

Figure 7: Geometric shape of water bridge

a. Axis of symmetry at r=0

Symmetry condition is applied at r=0. The flow velocity is zero in r direction and the shear stress is zero in z direction.

$$\boldsymbol{u} \cdot \boldsymbol{n} = \boldsymbol{0} \tag{23}$$

$$\left(-p\boldsymbol{I} + \mu(\nabla\boldsymbol{u} + (\nabla\boldsymbol{u})^T)\right) \cdot \boldsymbol{n} = \boldsymbol{0} \tag{24}$$

Where $\boldsymbol{n}$ is the outward normal vector.

b. Axis of symmetry at z=0

Symmetry condition is applied at z=0. The flow velocity is zero in z direction and the shear stress is zero in r direction.

$$\boldsymbol{u} \cdot \boldsymbol{n} = \boldsymbol{0} \tag{25}$$

$$\left(-p\boldsymbol{I} + \mu(\nabla\boldsymbol{u} + (\nabla\boldsymbol{u})^T)\right) \cdot \boldsymbol{n} = \boldsymbol{0} \tag{26}$$

c. Interface of liquid phase and gas phase

The stress will be balanced on the interface of liquid-gas. The equation is called stress balance equation for the existence of the static capillary surface.

$$\boldsymbol{n}_1\boldsymbol{T}_1 - \boldsymbol{n}_1\boldsymbol{T}_2 = \boldsymbol{\sigma}(\nabla_t \cdot \boldsymbol{n}_1)\boldsymbol{n}_1 - \nabla_t\boldsymbol{\sigma} \tag{27}$$

where $\boldsymbol{n}_1$ is the unit normal vector which points toward another fluid, $\boldsymbol{T}_1$ and $\boldsymbol{T}_2$ are the stress tensors, σ is the surface tension associated with the interface, and ∇_t is the surface gradient. $\nabla_t \cdot \boldsymbol{n}_1$ is twice the mean curvature of the surface.

$$\nabla_t = (\boldsymbol{I} - \boldsymbol{n}\boldsymbol{n}^T)\nabla \tag{28}$$

The relationship between mass flux and velocity in liquid and gas phase is described by Scardovelli and Zaleski [2.4].

$$\boldsymbol{u}_1 = \boldsymbol{u}_2 + M_f\left(\frac{1}{\rho_1} - \frac{1}{\rho_2}\right)\boldsymbol{n}_1 \tag{29}$$

Where $\boldsymbol{u}_1$ and $\boldsymbol{u}_2$ are the flow velocity in liquid phase and gas phase at liquid-gas interface, respectively. ρ_1 and ρ_2 are the density of liquid and gas, respectively. M_f is the mass flux.

d. Liquid-solid interface

The combination of the assumption Navier slip and the capillary force on wall is employed in the simulation. Navier slip introduce a friction on the liquid-solid interface.

$$\boldsymbol{F}_{fr} = -\frac{\mu}{\beta}\boldsymbol{u} \tag{30}$$

Where β is slip length whose value is normally 0.1 times the size of grid. The capillary force on wall adopt the Young's equation:

$$F_c = \sigma\cos(\theta_s) \tag{31}$$

Where θ_s is contact angle.

(2) Boundary conditions of mesh

In the control algorithm of moving mesh, the easiest way to control the mesh motion is to pre-specify the grid motion at the boundary and automatically solve the internal grid by using Laplace equation. The influence of the boundary conditions on the grid movement is gradually introduced into the interior to achieve grid computing and update.

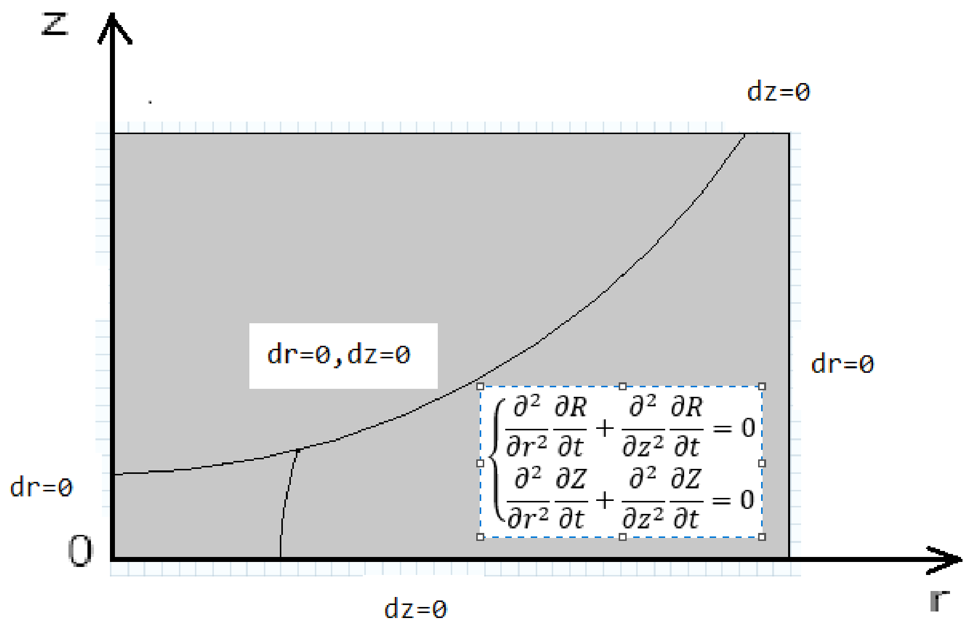

Figure 8: Mesh boundary conditions

The mesh boundary condition is showed in Figure 8. At r=0 and r=4mm, the prescribed mesh displacement is zero in z direction. At z=0 and z=2.5mm, the prescribed mesh displacement is zero in r direction. The prescribed mesh displacement is zero in both r and z direction at the surface of the ball.

Winslow smoothing is employed for the Laplace equation to update the internal grid. Therefore, the effect of mesh boundary conditions can be gently introduced into the internal grid so that the mesh is smoothly deformed.

$$\begin{cases} \frac{\partial^2}{\partial r^2}\frac{\partial R}{\partial t} + \frac{\partial^2}{\partial z^2}\frac{\partial R}{\partial t} = 0 \\ \frac{\partial^2}{\partial r^2}\frac{\partial Z}{\partial t} + \frac{\partial^2}{\partial z^2}\frac{\partial Z}{\partial t} = 0 \end{cases} \tag{32}$$

Where (R, Z) is the coordinate of mesh.

The velocity of mesh at liquid-gas interface is calculated by the equation:

$$\boldsymbol{u}_{mesh} = (\boldsymbol{u}_1 \cdot \boldsymbol{n}_1 - \frac{M_f}{\rho_1})\boldsymbol{n}_1 \tag{33}$$

3.4.2 Boundary conditions of Transport of Diluted Species

a. Gas-solid interface;

Symmetry condition is applied at r=0. The transport of diluted species is zero in r direction.

$$-\boldsymbol{n} \cdot (-D\nabla c) = 0 \tag{34}$$

b. Axis of symmetry at z=0;

Symmetry condition is applied at r=0. The transport of diluted species is zero in r direction.

$$-\boldsymbol{n} \cdot (-D\nabla c) = 0 \tag{35}$$

c. Liquid-gas interface;

The vapor concentration is assumed to be saturated near the liquid-gas interface. The experience equation [9] of the relationship between temperature near interface T_{in} and saturated pressure P_{sat} can be applied

$$P_{sat} = exp\left(9.487 - \frac{3.893\times10^3}{T_{in}+230.47}\right) \tag{36}$$

The saturated vapor pressure can be transferred to concentration by using ideal gas theory

$$c_{sat} = \frac{P_{sat}}{RT_{in}} \tag{37}$$

Where R is the ideal gas constant.

Outer boundary of gas phase

The vapor concentration is determined by the temperature and relative humidity.

$$c_\infty = c_{sat}H \tag{38}$$

Where H is relative humidity.

3.5 The setting of initial values

The rationality of initial values is important to the accuracy of the solution and the speed of convergence.

3.5.1 The initial value of Laminar Two-phase Flow, Moving Mesh

The initial value of velocity is zero in both liquid phase and gas phase.

$$\boldsymbol{u}_{t=0} = \boldsymbol{0} \tag{39}$$

The initial value of displacement of mesh is zero.

$$dR_{t=o} = 0, dZ_{t=0} = 0 \tag{40}$$

The initial pressure is zero. In this situation, the pressure is relative pressure of liquid phase and gas phase. It is easy to observe the weak difference of pressure during the evaporation.

$$P_{t=0} = 0 \tag{41}$$

3.5.2 The initial value of vapor concentration

The initial value of vapor concentration is set as the vapor concentration of the environment.

$$c_{t=0} = c_{sat}H \tag{42}$$

3.6 Other settings

3.6.1 The discrete methods

There are three types of discretization methods to control the type of discrete element of finite element method, P1+P1, P2+P1, and P3+P2.

P1+P1 implies that the velocity component and pressure fields are both linear elements. Compared to element of higher order, it possesses the characteristics of higher speed of calculation and lower tendency to spurious resonance. However, its accuracy is lower.

P2+P1 implies that the velocity component is described by second-order element, while the pressure field is linear.

P3+P2 implies that the velocity component is third-order element, while the pressure field is second-order element. It possesses the highest accuracy. However, it takes long period of time to calculate.

Considering the integrated model, the velocity field and the pressure field are more of concerned. After the balance of computational efficiency and accuracy is considered, P2 + P1 discretization method is adopted.

3.6.2 The mesh

Figure 9 shows the schematic of the mesh. The free triangular mesh is easier to adapt to the boundary than free quad mesh, and the solution is easier to converge. The mapped mesh is built inside the water bridge to avoid the singularity and deformation of free interface near the liquid-gas interface. The maximum element size of mapped mesh is 0.02mm.

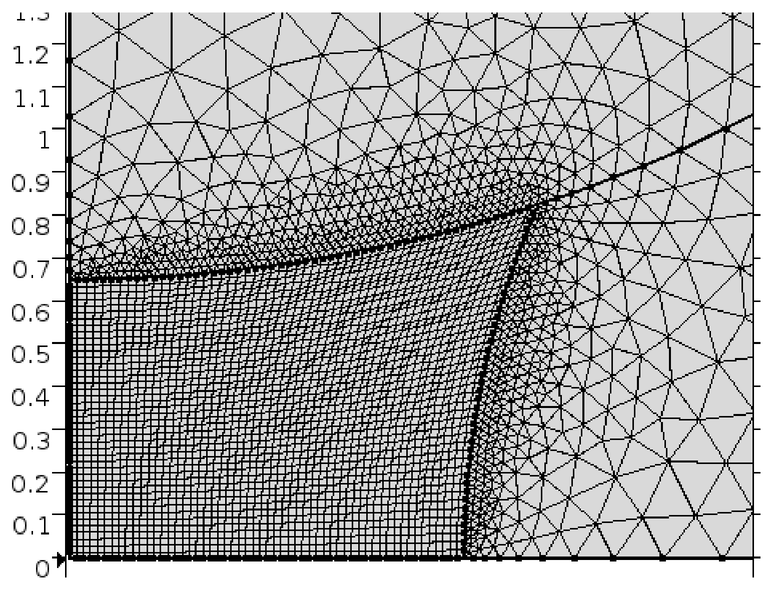

Figure 9: Typical mesh in the water bridge and its vicinity

4. Results and discussions

In what follows we examine the results of simulations under two sets of approximations. In the first one, defined as Interface Driven solution, the variable shape and the position of the (liquid – gas) interface is the driving variable. In other terms, a circular interface is imposed at a specific time interval or the total volume of the liquid, by defining the radius of the contact and the radius of the gorge, following as closely as possible the experimental results. In particular, the point of triple contact is imposed as in the experiment, without explicit requirement of pinning. This is a serious advantage, because at the current settings of the routine, the Navier frictional conditions on liquid-solid interface tacitly imply no displacement of the triple contact point. This is a serious limitation, because as experimentally shown by Mielniczuk et al., 2015, the contact line undergoes initially some pinning, followed by the contact displacement, followed again by pinning. Experimental conditions are summarized by Mielniczuk et al., 2013, 2014 and 2015. At the initial moment the interface vapor/liquid flux is not imposed. Instead liquid flux is implicitly determined by the difference in liquid volume between two adjacent positions of the interface. The solution consists of the Laplace pressure distribution along the interface.

4.1 Interface driven solution: static snapshots

4.1.1 Pressure distribution along the contour

The starting point are the experimental results placed in the Appendix and consisting in the geometry of the interface. Laplace pressure values were also experimentally determined at z = 0, 1/3h, 2/3h, and h, where h is the variable vertical position of the triple point. These results (unpublished) were obtained at LMGC (Laboratoire de Mécanique et de Genie Civil) of the University of Montpellier, France (Dr. Bolo Mielniczuk and Professor Saïd Youssoufi) in collaboration with Duke University (Professor Tomasz Hueckel). The experimental Laplace pressure has been calculated from the Laplace-Young equation, from prior point-wise measurements of the principal (normal) curvatures at the experimental interface.

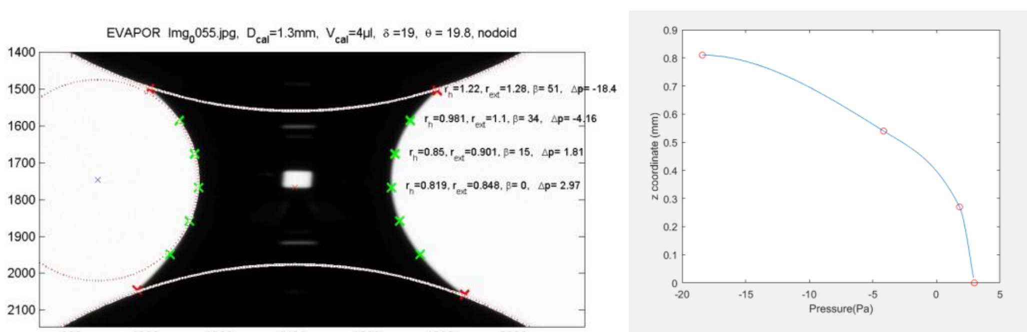

(a)

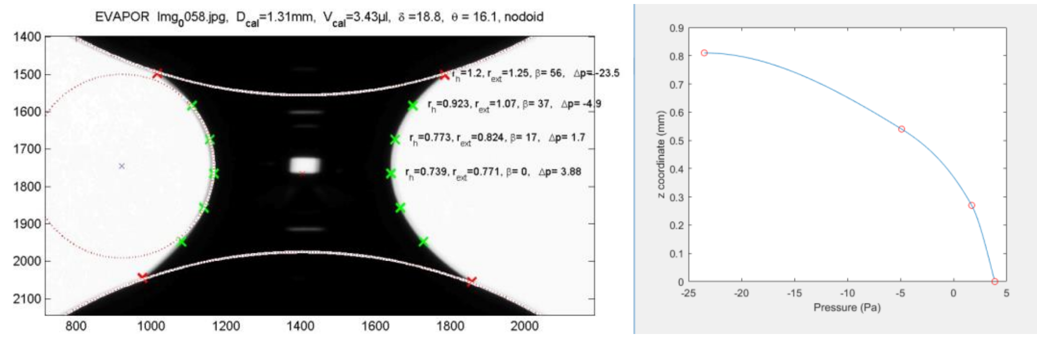
EVAPOR Img$_0$058.jpg, D_{cal}=1.31mm, V_{cal}=3.43µl, δ =18.8, θ = 16.1, nodoid
r_h=1.2, r_{ext}=1.25, β= 56, Δp= -23.5
r_h=0.923, r_{ext}=1.07, β= 37, Δp= -4.9
r_h=0.773, r_{ext}=0.824, β= 17, Δp= 1.7
r_h=0.739, r_{ext}=0.771, β= 0, Δp= 3.88
z coordinate (mm)
Pressure (Pa)

(b)

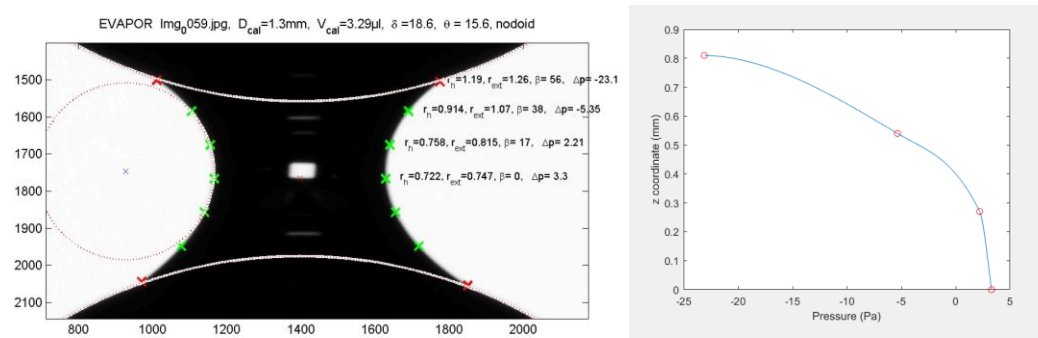
EVAPOR Img$_0$059.jpg, D_{cal}=1.3mm, V_{cal}=3.29µl, δ =18.6, θ = 15.6, nodoid
r_h=1.19, r_{ext}=1.26, β= 56, Δp= -23.1
r_h=0.914, r_{ext}=1.07, β= 38, Δp= -5.35
r_h=0.758, r_{ext}=0.815, β= 17, Δp= 2.21
r_h=0.722, r_{ext}=0.747, β= 0, Δp= 3.3
z coordinate (mm)
Pressure (Pa)

(c)

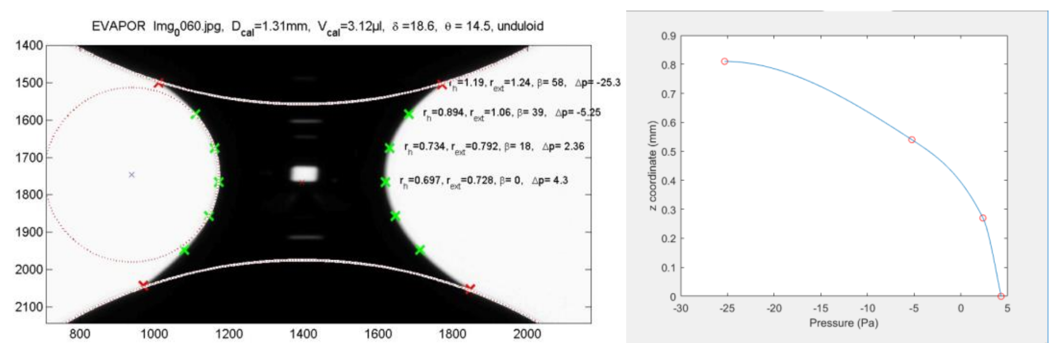
EVAPOR Img$_0$060.jpg, D_{cal}=1.31mm, V_{cal}=3.12µl, δ =18.6, θ = 14.5, unduloid
r_h=1.19, r_{ext}=1.24, β= 58, Δp= -25.3
r_h=0.894, r_{ext}=1.06, β= 39, Δp= -5.25
r_h=0.734, r_{ext}=0.792, β= 18, Δp= 2.36
r_h=0.697, r_{ext}=0.728, β= 0, Δp= 4.3
z coordinate (mm)
Pressure (Pa)

(d)

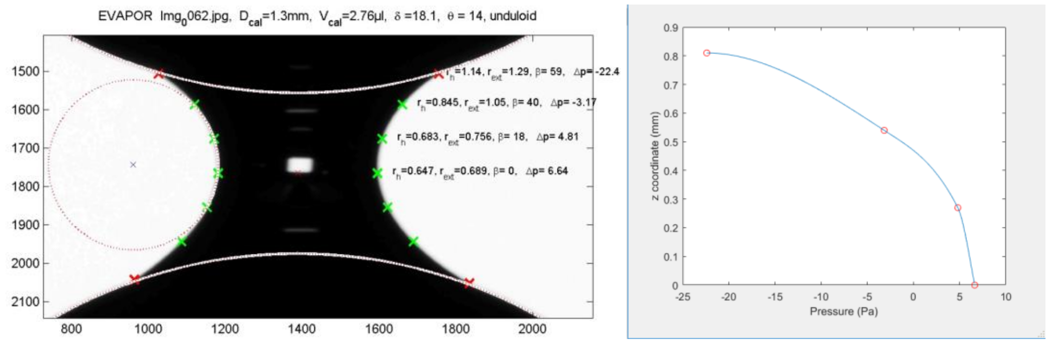

(e)

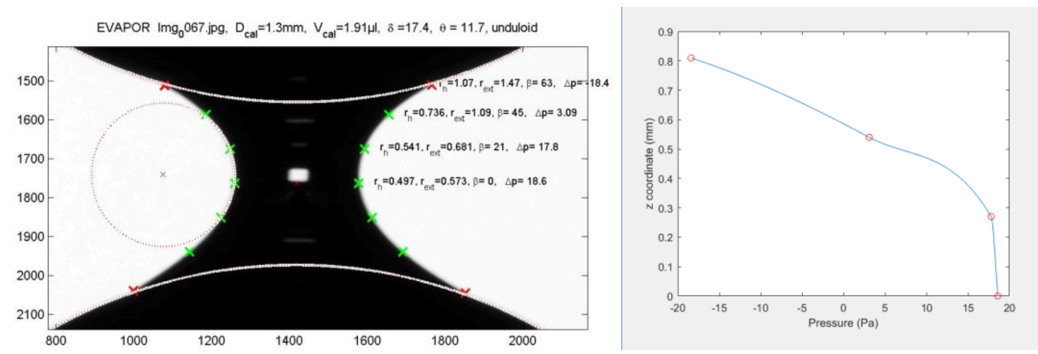

(f)

Figure 10: The geometry of water bridge and their pressure difference distribution along free interface at about 4μl, 3.4μl, 3.2μl, 3.1μl, 2.8μl, and 1.9μl, respectively

Figure 10 shows the geometry of water bridge, i.e. its interface profile and the Laplace pressure distribution along free interface from center to the three-phase contact line at about 4μl, 3.4μl, 3.2μl, 3.1μl, 2.8μl, and 1.9μl, respectively. The most important observation is the highly non-uniform distribution of the Laplace pressure ranging in the initial situation from positive pressure of 3Pa at the center to – 19 Pa at the triple contact. Therefore, there is a significant suction effect at the three-phase contact line.

The position of the interface and its geometry has been fed as input to the COMSOL Multiphysics software for 6 different consecutive configurations. As the experimental data correspond to those from the process activated by evaporation flux across the interface, they clearly do not correspond to the situation of equilibrium. The obtained results correspond to the situation in which there is no external flux, while the flow of liquid and gas are such that satisfy the interface equilibrium condition. The resulting pressure distribution along the interface imparts the Navier-Stokes flow within the water body.

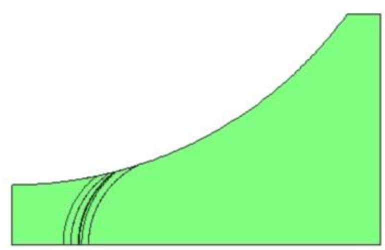

(a)

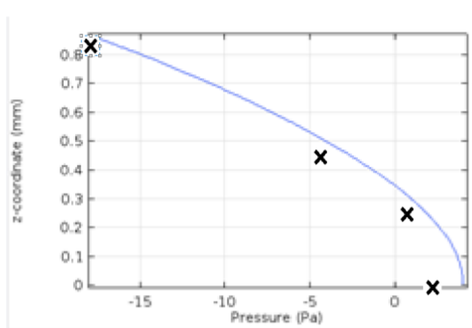

(b)

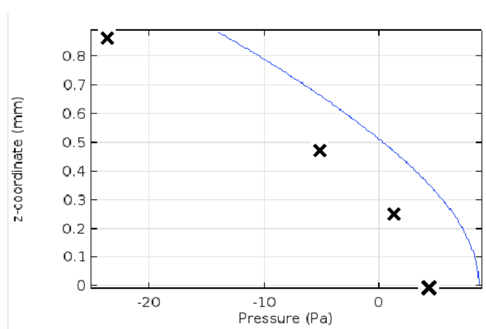

(c)

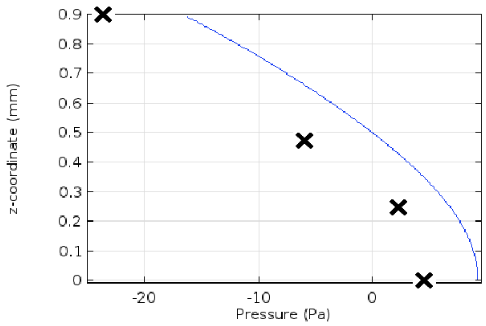

(c)

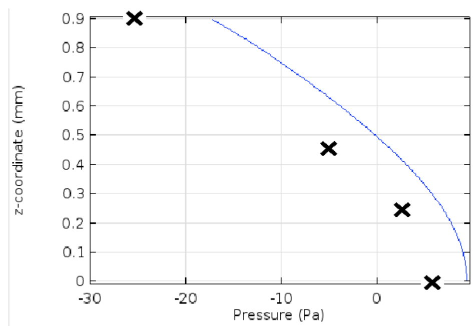

(d)

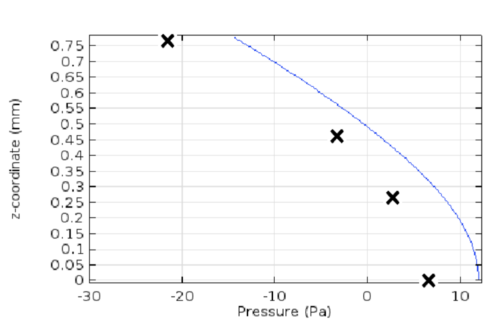

(e)

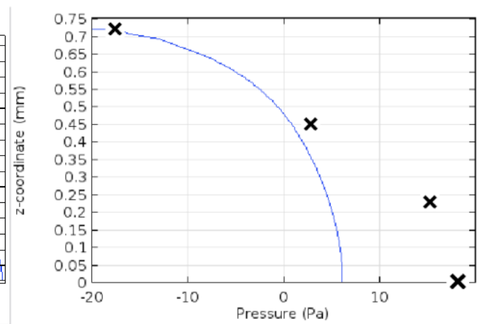

(f)

Figure 11: (a) The geometry of water bridge at 4μl, 3.4μl, 3.2μl, 3.1μl, 2.8μl, and 1.8μl; (b)-(g): The pressure distribution along free interface at4μl, 3.4μl, 3.2μl, 3.1μl, 2.8μl, and 1.8μl, respectively

Figure 11(a) shows the sequence of the interface configurations at 4μl, 3.4μl, 3.2μl, 3.1μl, 2.8μl, and 1.8μl of total liquid volume, while the Laplace pressure difference distribution along the free interface which is calculated by the software is presented in Fig. 11(b). The cross represents the experimental result that is calculated by Laplace theory. The geometry of water bridge is constructed according to the geometry of the experiment, which means these are the static results without considering the influence of the evaporation flux. It is found that the pressure from the middle of the bridge to the contact goes from positive to negative values along the contour of free interface. This is not far from the actual pressure distribution data from the experiments. It is worth noting that the calculations are conducted ignoring the hydrostatic effect. At the center of the bridge the water column is about 0.7 mm high, which is equivalent to an extra pressure of 7 Pa, which would shift the data toward more positive value at the lower part of the graph.

4.1.2 Pressure distribution within the water bridge

The interface pressure distribution constitutes boundary conditions for the pressure field across the bridge itself.

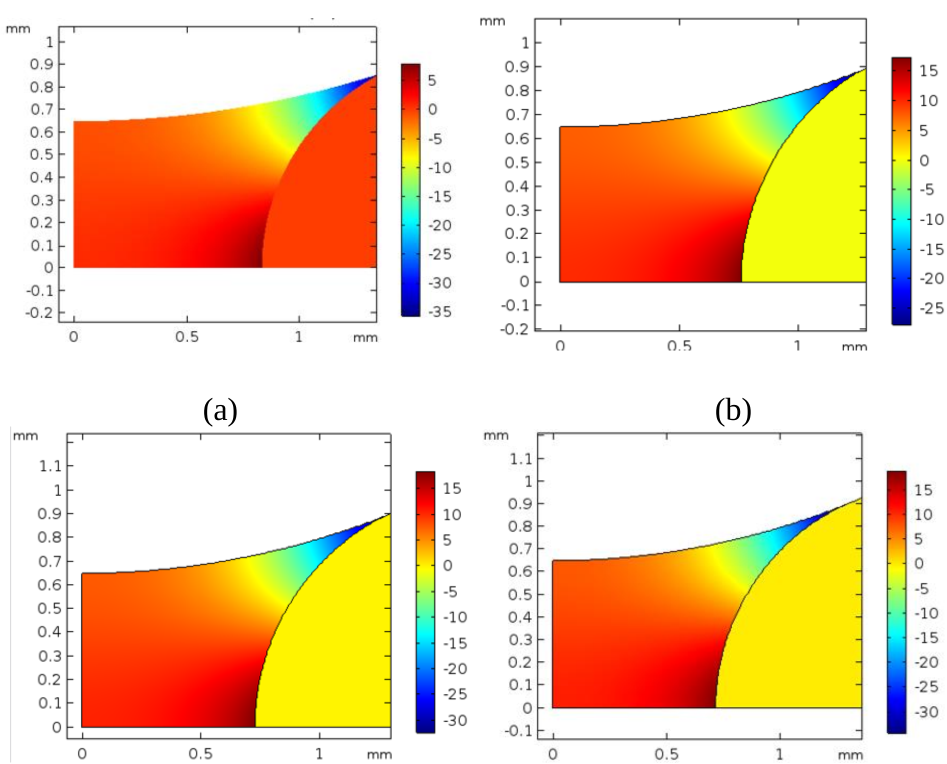

(a) (b)

(c) (d)

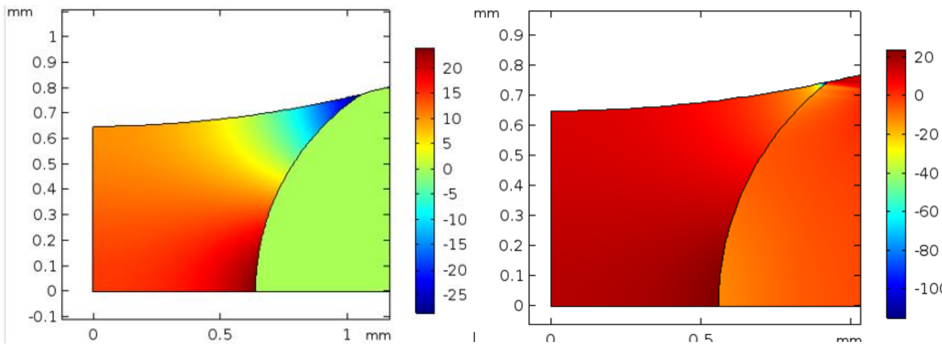

(e) (f)

Figure 12: The pressure distribution inside the water bridge at 4μl, 3.4μl, 3.2μl, 3.1μl, 2.8μl, and 1.8μl, respectively

Figure 12 shows the resulting of pressure distribution inside the water bridge at 4μl, 3.4μl, 3.2μl, 3.1μl, 2.8μl, and 1.8μl, respectively. The pressure is maximum at the center edge of the water bridge with positive pressure and minimum at the three-phase contact line with negative pressure. These solutions represent well the experimental results. The overall pressure within the bridge corresponds to the general results of Mielniczuk et al., 2015, in which positive values were measured for the particular separation of 1.3 mm, based on mid-height curvatures.

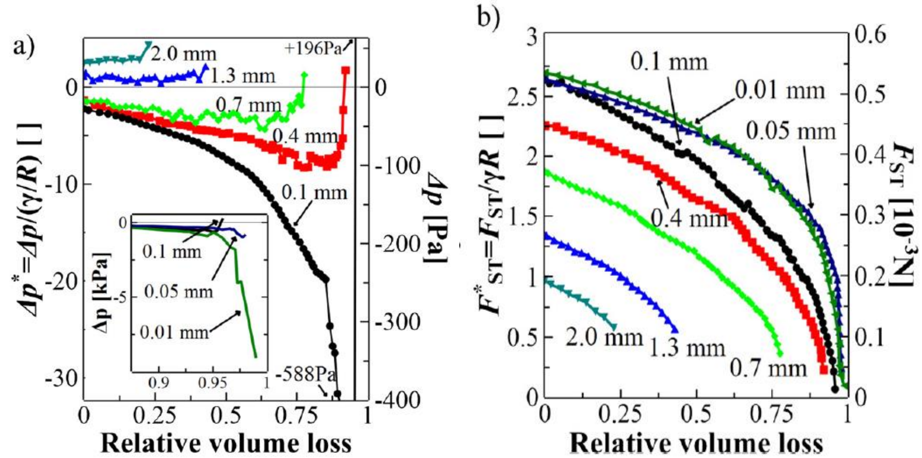

Figure 13: (a) Laplace pressure difference evolution for different separations; (b) Resultant surface tension force (after Mielniczuk et al. 2015) [15]

The negative pressure near the grains toward the triple line can be interpreted as a suction effect producing an attraction pulling the two grains closer. In a sense, in this continuum representation it depicts the effect of surface tension force, which is acting at the interface, but clearly cannot be represented in a continuum model. The resultant force of such surface tension is shown in Figure 13(b) to monotonically decrease during evaporation, as the intensity of negative pressure zone decreases with volume loss in Figure 12. Although this simulation explicitly ignores the effect of vapor flux distribution, the former is represented by the shape of the interface. The very strong concentration of the flux (see Figure 16) near the edges of the bridge logically results in the suction in the liquid phase near the triple point. Such concentration of the flux near the edges is also seen in the evaporation of the sessile droplets (Larson and Hu [2]).

The last calculated result concerning the pressure distribution at 1.8 μl shows a departure from the previous trend with a much narrower zone of suctions near the triple point. However, as easily seen in Fig. 13, the average bridge of separation of 1.3mm ruptures at an average volume of water of 2.25 μl. The rupture of bridges has been discussed in detail by Mielniczuk et al. [15].

4.1.3 Flow field

The fluid pressure field suggests strong pressure gradients across the bridge, which in turn suggests an intense Navier-Stokes flow.

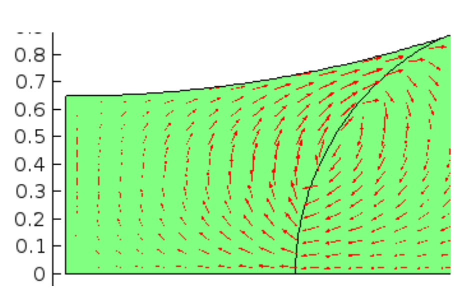

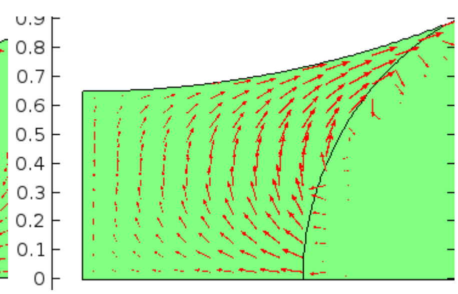

(a) (b)

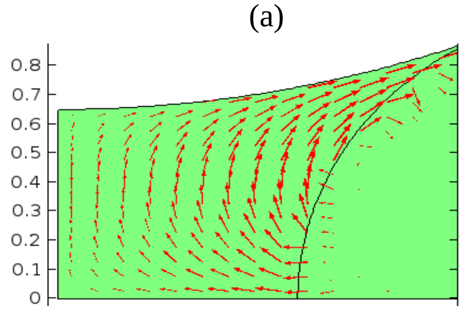

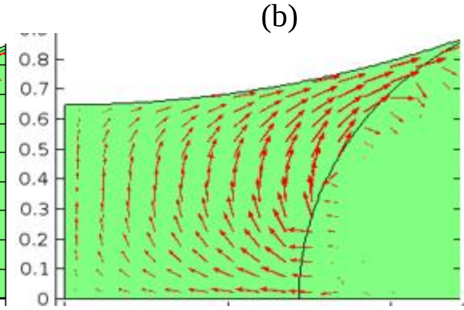

(c) (d)

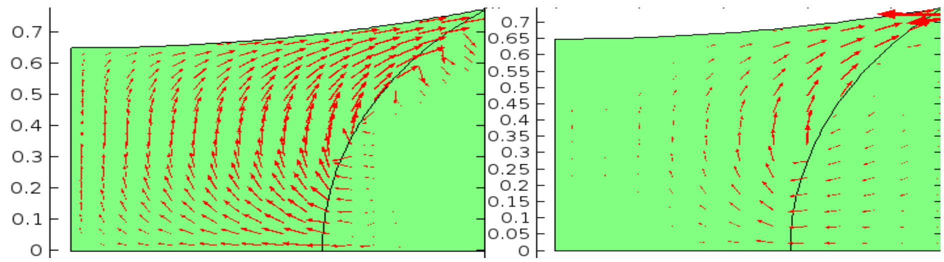

(e) (f)

Figure 14: The flow field inside the water bridge at 4μl, 3.4μl, 3.2μl, 3.1μl, 2.8μl, and 1.8μl, respectively

Figure 14 shows the flow field inside the water bridge at 4μl, 3.4μl, 3.2μl, 3.1μl, 2.8μl, and 1.8μl, respectively. These flow fields are induced by the interface pressure distributions that are calculated by Laplace theory. The closer to the free interface, the lager the flow velocity is. In general, water flows from the center of water bridge toward the solid/liquid interface and toward the three-phase contact line. For our considerations the most relevant conclusion is that for large portion of the process the flow along the liquid-solid interface is directed against the motion of the triple contact line. The intense flow along the solid surface toward the triple contact line coincide with the concentration of the vapor flux at the edge of the bridge, Fig. 16, as already mentioned with respect to the concentration of suction.

In a sense, this motion counteracts the contact line pinning. Notably, even if the solution for each step is conditioned of the immobile contact point, the fact that we allow the interface to intersect the solid surface close and closer to the axis of the bridge, effectively allows for the pinning and depinning, as observed experimentally. This flow field can bring the particles from the center of water bridge to the three-phase contact line (coffee-ring effect). The flow within the evaporating bridge has been seen in the experiments (See Movie 1)

To conclude the discussion on the cycle of the Interface Driven solution results, it is found that as the results are relatively close to the experimental ones regarding the Laplace pressure, the pressure field within the water body, and the character of the flow, the approximation, on which the solution is based, i.e. neglecting the effect of evaporation flux and recognizing the motion of the interface as the principal source of inducing the flow within the bridge is an acceptable approximation.

4.2 Evaporation flux driven solution: dynamic results

4.2.1 Vapor concentration

The evaporation process is assumed as driven by diffusion of vapor in the air, between saturation concentration at the interface with water and an ambient level at an assumed distance [18]. Deegan's [1]and Hu's in their classical paper [2] considered the evaporation of a droplet assuming its shape as a spherical cap. In this study, due to the special and variable geometry of water bridge, the distribution of concentration around the water bridge is not uniform. "Transport of Diluted Species" (TDS) module of COMSOL Multiphysics is employed to obtain the vapor concentration distribution. However, the form of the liquid/gas interface is calculated from a separate coupled COMSOL module "Two-phase laminar flow, moving mesh" (2-PLF). The two modules feed one to another as follows: the original (experimental) interface is pre-imposed to TDS which calculates the vapor flux at the interface corresponding to a time step, 0.001s. This flux is fed to 2-PLF which in turn produces as one of the results a new geometry of the interface. The new interface geometry is then fed again to TDS, which produces a new flux for another time step, and so on.

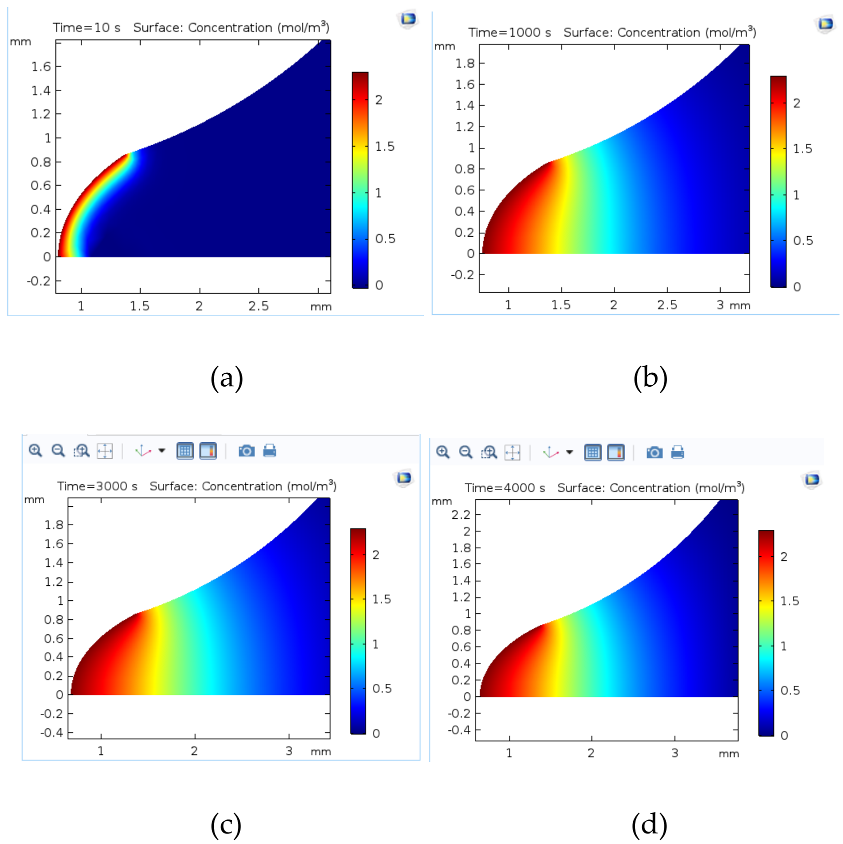

Figure 15: Evolution of vapor concentration distribution in gas around the capillary bridge at t=10s, t=1000s, t=3000s and t=4000s

Figure 15shows the evolution of vapor concentration around water bridge at selected time periods. The diffusion constant of water vapor is 0.0016mm²/s. The interface evolution is constrained by the inexplicit condition that the contact point of solid/liquid/gas interface remains fixed (pinning). The resulting contact angle varies (decreases) slightly (which is not in accordance with Laplace law [14]). Another inexplicit assumption in the software is the evolution of the interface into a circle and a tangent short straight segment connecting to the contact point.

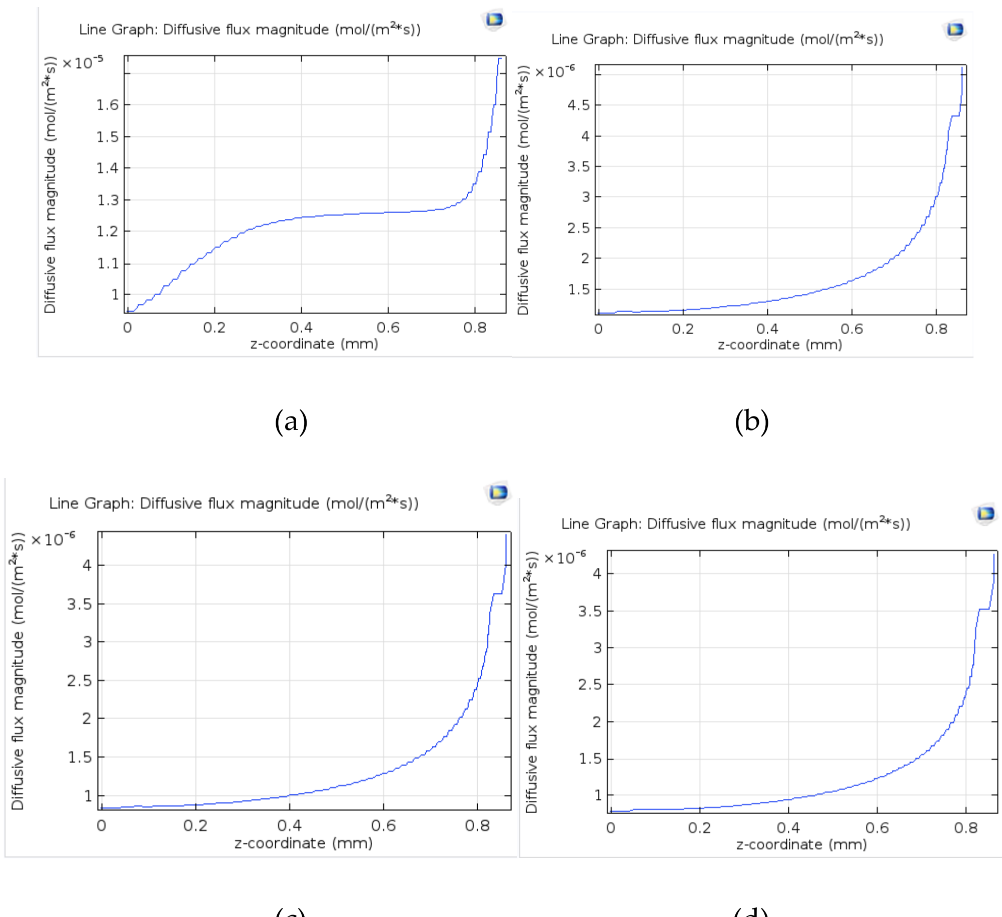

Figure 16: (a)- (d) Diffusive flux of vapor along the contour of water bridge (Evaporation flux) at t=10s, t=10s, t=1000s, t=3000s and t=4000s

Figure 16 shows the diffusive flux (hence evaporation flux) of vapor along the contour of water bridge. The diffusive flux changes with the geometry of water bridge evolving with time and water volume loss. However, the change in the flux is very small over the course of the process. The common characteristic is that the diffusive flux is relatively low in the middle of water bridge and very high at the edge of the water bridge. Interestingly, a perturbation near the edge appears to be linked to the aforementioned tangency point between the circle and the straight segment of the interface.

4.2.2 Pressure of the re-equilibrated configuration

The simulation of the entire process is conceived as follows. The initial situation needs a specification of the interface of an equilibrium capillary state, that is a fictitious state prior to the onset of evaporation. It is a fictitious state because requires a uniformly humid external environment. As an initial state the interface surface was as previously imposed as close as possible to the experimental one. However, as such surface is not necessarily corresponding to the theoretical equilibrium configuration, the initial response of the software was to find such theoretical configuration. That implies activation of flow and reconfiguration of the interface pressure. Fig. 17

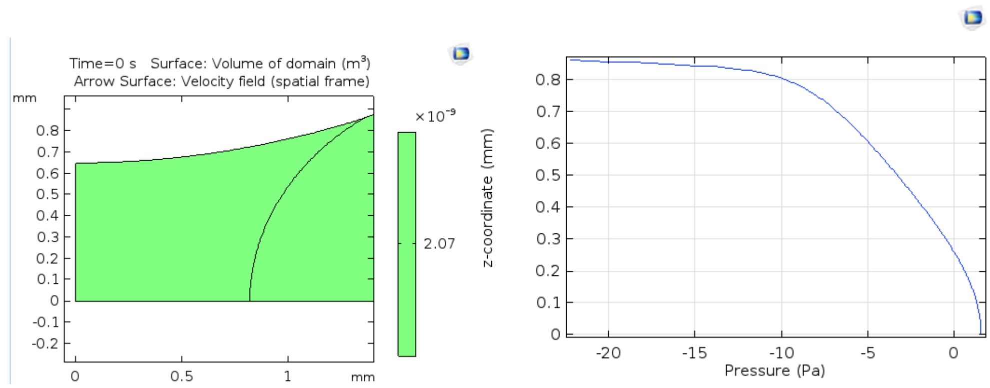

Figure 17: Initial geometry and the corresponding pressure distribution along the free interface

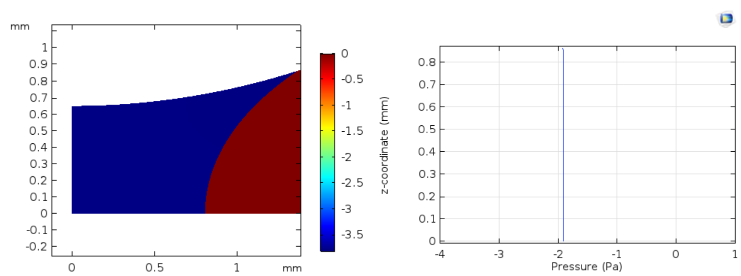

(a)

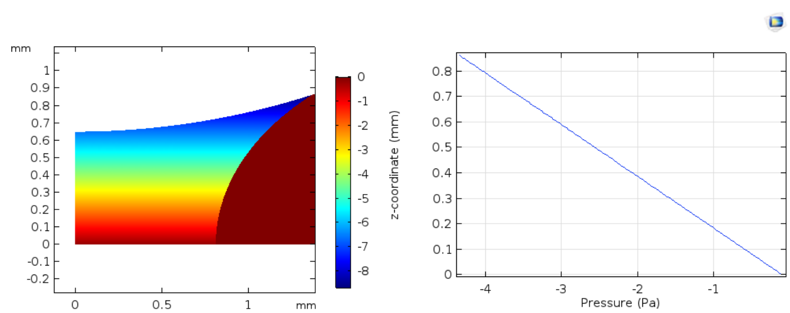

(b)

Figure 18: Re-equilibrated geometry and the corresponding pressure distribution along the free interface (a)without weight (b)with weight

Figure 17 shows the initial interface shape and the corresponding pressure at the interface prior to equilibration procedure. As seen the pressure is the same as in the initial solution of Figure 11(b). Fig. 18 shows the re-equilibrated interface shape and the corresponding pressure at the interface after the equilibration procedure. As seen the pressure for a weightless water is constant and negative (ab. -1.90 Pa) over almost entire height. This is clearly less than the positive value of the mean (over several experiments) initial pressure of about 11 Pa for the 1.3 mm bridge shown in Fig. 13a and calculated from the average curvatures at the gorge of the bridge. The value of the pressure at the gorge of the experiment shown in Fig. 1a is about 3.88 Pa. The re-equilibrated solution with the weight yields the pressure linearly changing with the height and reaches the value at the gorge of -0.1 Pa. The negative values of pressure in both cases imply that the bridge is acting with an attractive force on the grains.

The shape of the adjusted interface, shown in Fig. 18a appears not to be a circle, but rather composed of a straight segment anchored at the original triple point and a tangent circle which produces the initial gorge radius of 0.79mm, as opposed to the experimental one of 0.819 mm (see Fig. 10a). Notably, as a result of the adjustment the initial volume of the bridge has changed to 4.14 μl.

The next step in the simulation is the application of the evaporation flux at the interface. As mentioned before, the flux is converted to an equivalent liquid flux. This process is realized in time steps by the software. The minimum one is 0.001 sec., the maximum is 0.1 sec. The results of the simulations are reported below.

4.2.3 Flow field results

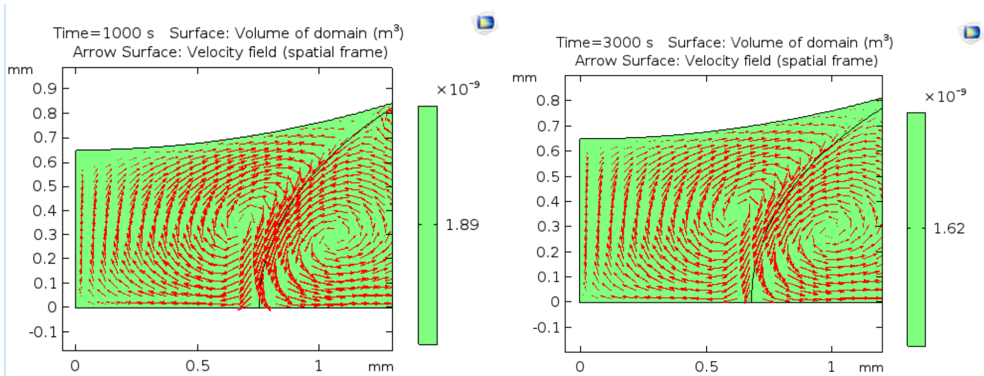

Figure 19: Flow field inside the water bridge at t=1000s (V=3.78 μl) and t=3000s (V=3.24 μl)

Figure 19 shows the flow field inside the water bridge. As opposed to the previous solution, the interface is pinned at the original point of contact of the three phases, as a fixed boundary condition. The displacement of the interface pushes the liquid near the free interface to flow from three phase contact line toward the middle of the water bridge, first along the free interface. The liquid flow forms a cell with a clockwise rotation.

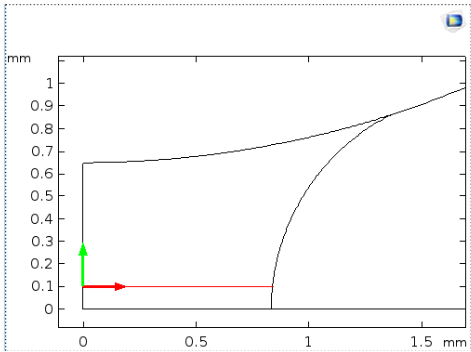
mm
1.5 mm

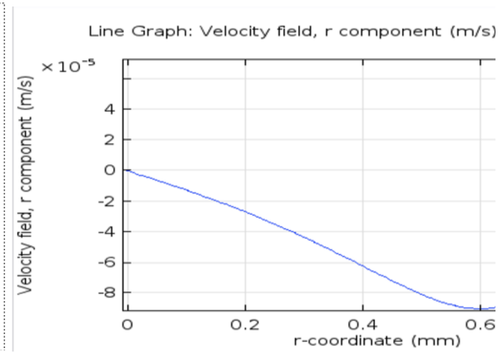
Line Graph: Velocity field, r component (m/s)
×10⁻⁵
Velocity field, r component (m/s)
r-coordinate (mm)

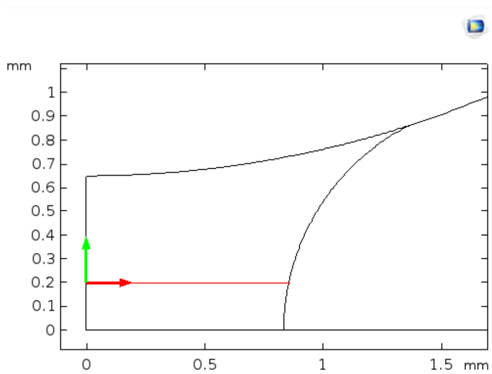
mm
1.5 mm

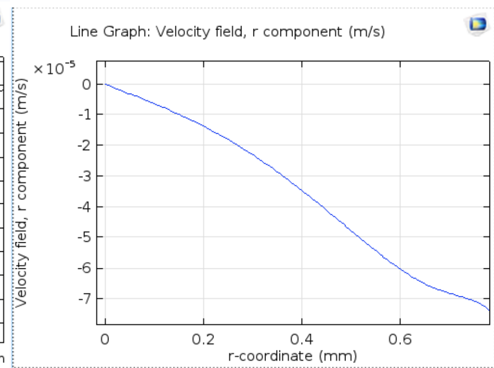
Line Graph: Velocity field, r component (m/s)
×10⁻⁵
Velocity field, r component (m/s)
r-coordinate (mm)

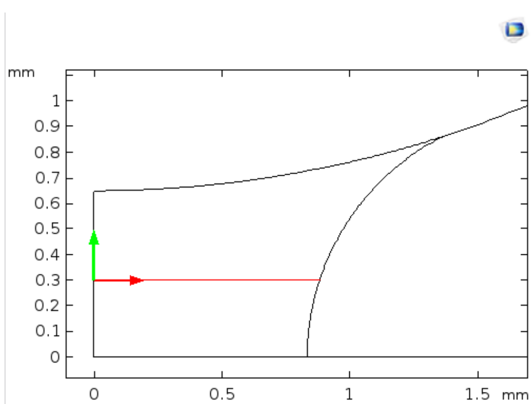
mm
1.5 mm

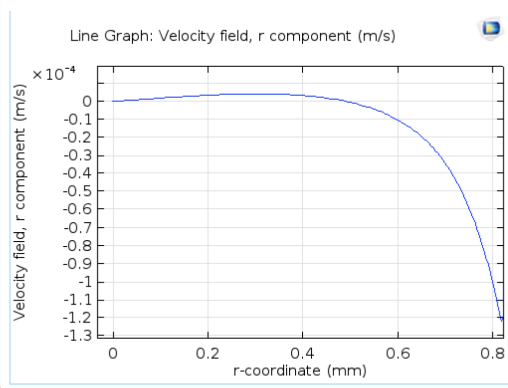
Line Graph: Velocity field, r component (m/s)
×10⁻⁴
Velocity field, r component (m/s)
r-coordinate (mm)

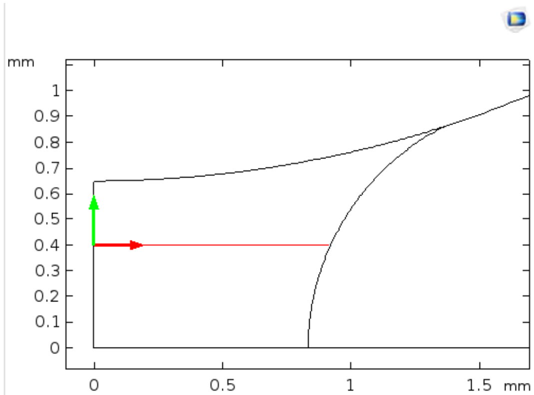

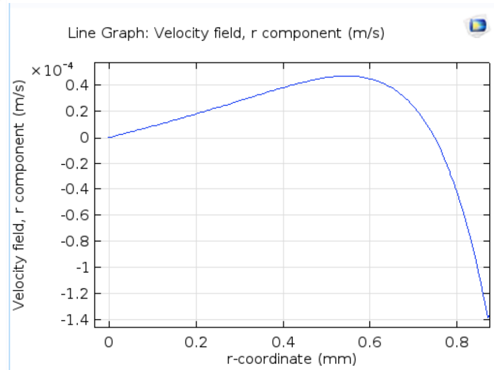

Line Graph: Velocity field, r component (m/s)
Velocity field, r component (m/s)
r-coordinate (mm)

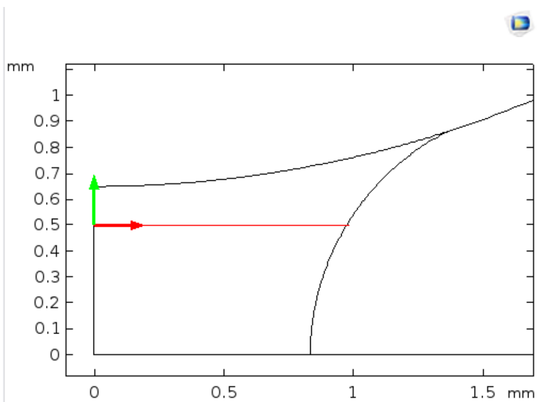

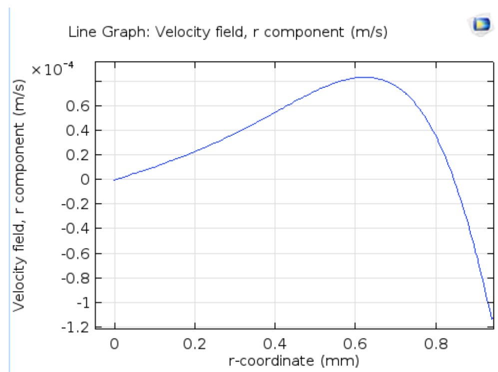

Line Graph: Velocity field, r component (m/s)
Velocity field, r component (m/s)
r-coordinate (mm)

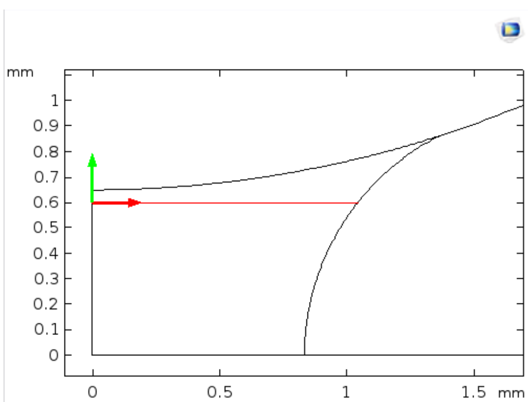

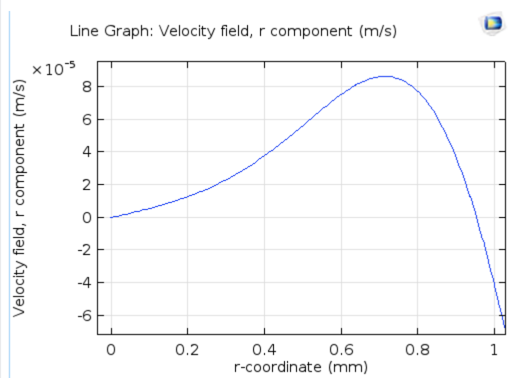

Line Graph: Velocity field, r component (m/s)
Velocity field, r component (m/s)
r-coordinate (mm)

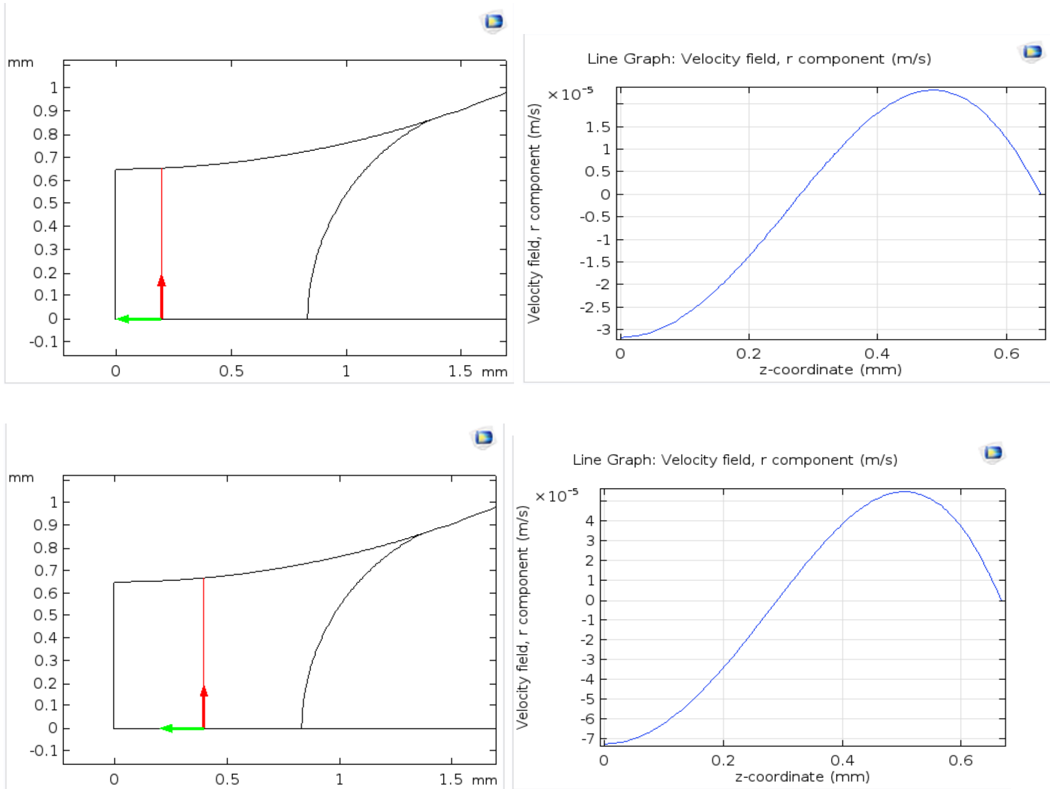

Figure 20: Velocity of flow along the radial and vertical cross sections indicated at t=1000s

The radial components of velocities in a series of cross-sections are shown in Figure 20. The flow is very slow in the middle of the bridge and relatively faster near the free interface. The maximum value at 1000sec. is about 0.1 mm/s.

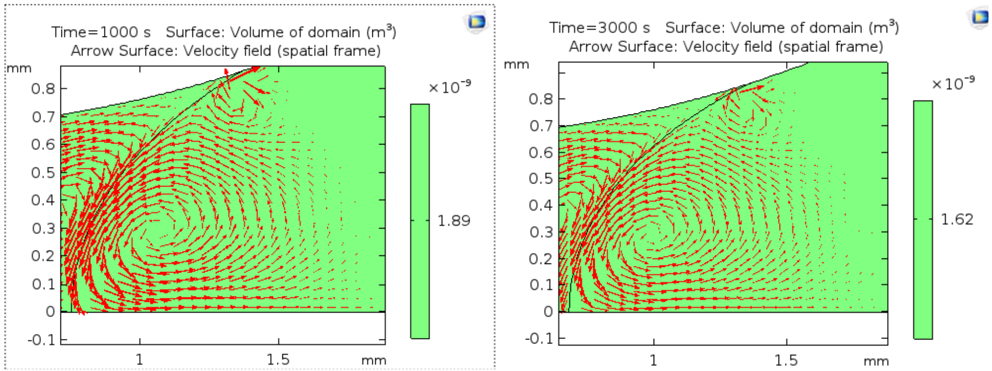

Figure 21: Flow field outside the water bridge at t=1000s and t=3000s

Figure 21 shows the flow field in the gas phase. The gas flow is induced by the movement of free interface. The gas flows counter-clockwise from a region near the three-phase contact line toward the middle of water bridge along the free interface.

4.2.4 Result of pressure distribution

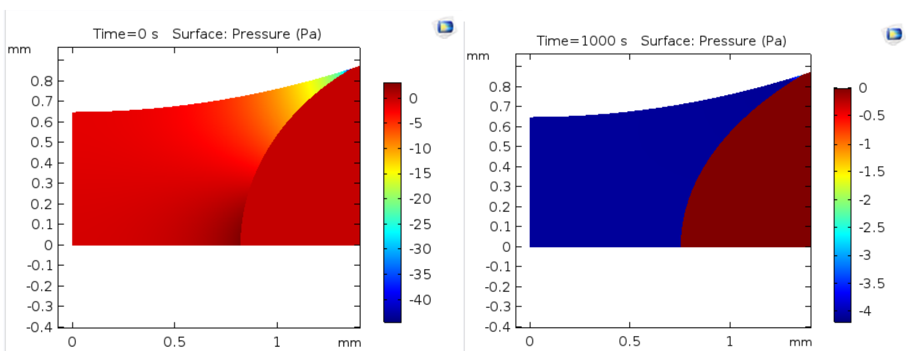

(a) (b)

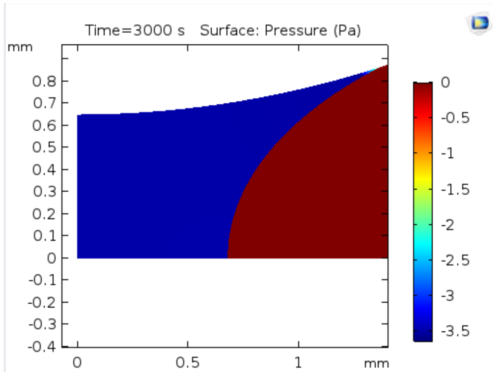

(c)

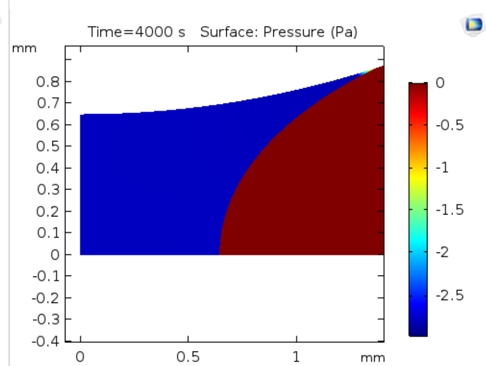

(d)

Figure 22: Pressure distribution inside the water bridge at t=0s, t=1000s, t=3000s and t=4000s, respectively

Figure 22 shows the pressure distribution inside the water bridge. The pressure that is discussed in this paper is the relative pressure. The initial pressure is negative and minimum near the three-phase contact line. Clearly this is a non-equilibrated solution. When the evaporation takes place, the pressure maintains the negative value and becomes nearly constant across the almost entire field. There is visible decrease in suction near the three-phase contact line.

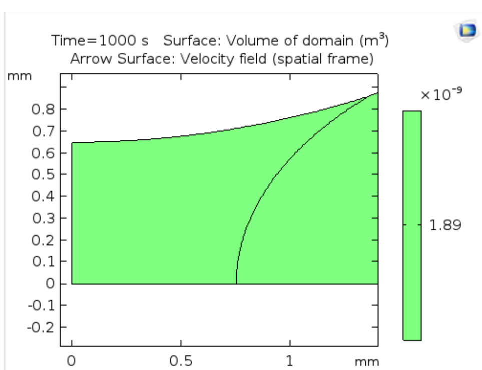

(a)

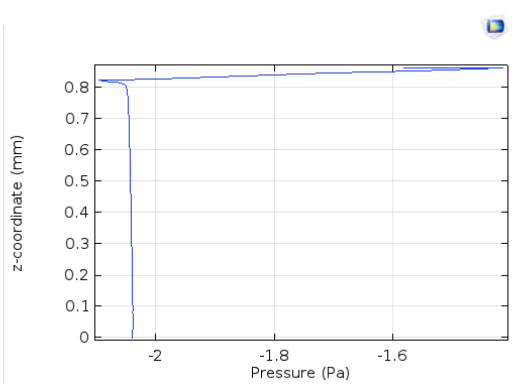

(b)

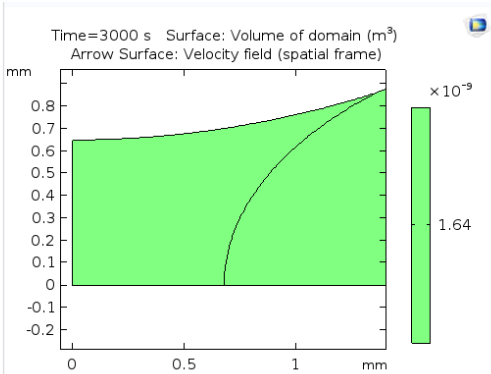

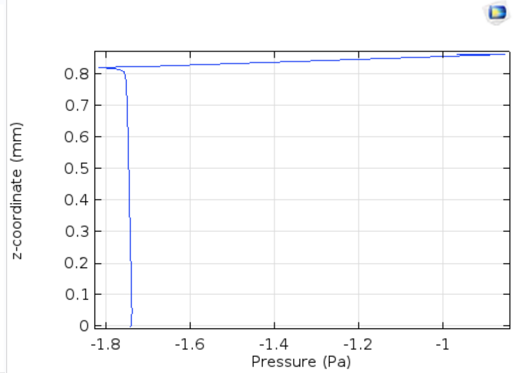

(c) (d)

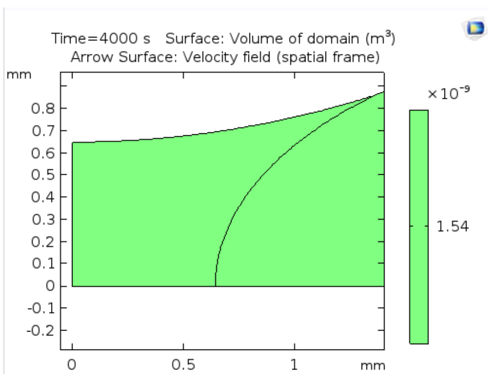

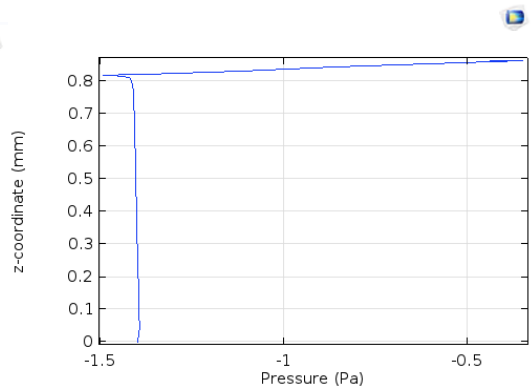

(e) (f)

Figure 23: The pressure distribution along the free interface at t=1000s

The pressure distribution along the contour of water bridge is shown in Figure 23. The pressure is negative throughout with a minimum at the center of the water bridge and maximum at the three-phase contact line. However, the pressure distribution is very different from the values obtained from the experiment calculated from Young-Laplace law using the local principal curvatures, shown in Figure 11. The experimental pressure is lower (in fact, it is suction) at the three-phase interface and higher (and positive) in the middle of the water bridge. The negative pressure inside the water bridge produces an effect to pull the two grains closer.

The striking features of the dynamic pressure difference are: the pressure is almost uniform across the bridge; there is a pressure singularity a short distance from the triple point, and finally there is a sharply different (nearly linear) distribution of pressure at the segment near the triple point. These three peculiarities throw in doubt the quality of the obtained solution.

Although the flow field of static solution is similar to the flow field of dynamic solution, the geometry of water bridge and pressure distribution exhibit obvious difference between static solution and dynamic solution. The difference between dynamic solution and static solution indicates that the stress is influenced by other factors. Not having access to the assumptions behind the details of the solutions, one can only provide hypothetical arguments regarding the obtained result. First, one can observe that the pinning of the triple line is imposed on the solution. There is no option of the free motion of the triple point. However, the experimental literature is filled with examples of depinning and repinning of the triple point during drying and displacements of sessile drops. (De Gennes et al. [19], Bormashenko [20])

Indeed, Afkhami et al. [21] underline a paradox of many solution with a contact line moving along no-slip or Navier contact type boundary conditions solid surface for sessile drops.

The discussed experiment shows indeed an initial pinning, depinning and repining (see also Mielniczuk et al., 2015) of the triple point during drying. Second, because of the imposed pinning the geometry of the interface is constrained, and visual inspection clearly shows a departure from the circular shape and visible flattening of the profile curve. Notably the curvature of the interface profile controls the ability to generate a negative component of the pressure. It seems that a choice of the geometrical characterization of the curve in the software leads to a substantial limitation of that ability. Thus the resulting negative pressures are drastically underestimated. The aforementioned singularity of the interface pressures in the dynamic solution testifies to the discontinuity of the curvature at the apparent point of intersection of two different curves used by the software in simulation of the interface. It emphasizes the crucial role of the precision required in reproducing the negative curvature of the interface. It appears in addition that in the dynamic simulation, it assumed that the entire field is assigned a constant pressure corresponding through the Laplace-Young equation as calculated from curvatures at the bridge gorge. If this is true, then the experimentally observed high gradients in interface pressures cannot be modelled with the dynamic routine of COMSOL.

Afkhami et al. [21] produced a numerical methodology to avoid messh dependence and a number of paradoxes in the solution with the moving interface. However, the methodology is based on a piecewise linear approximation of the interface near contact. As mentioned above excludes a probability of modeling suction near the contact which is observed in the experiments

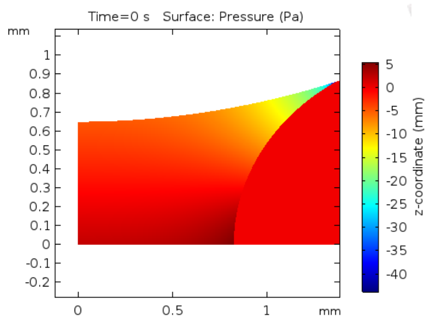

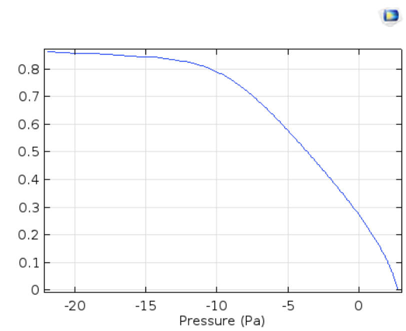

(a) (b)

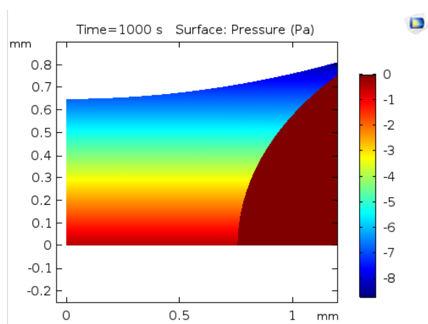

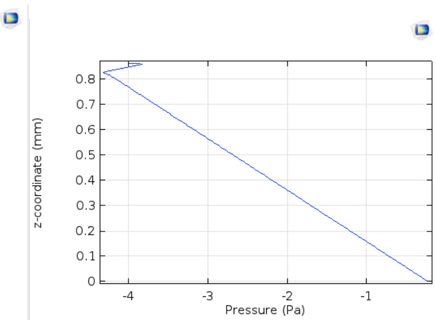

(c) (d)

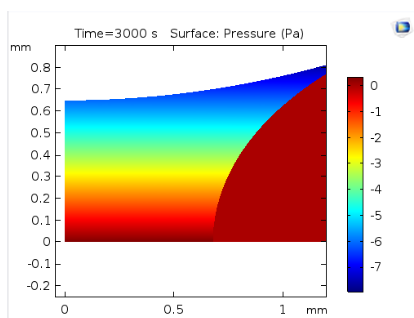

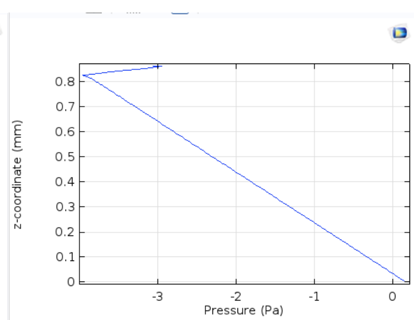

(e) (f)

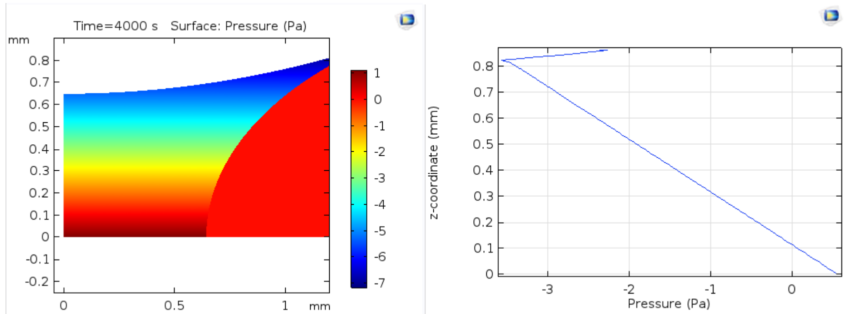

(g) (h)

Figure 24: (a), (c), (e), (g): The pressure distribution inside the water bridge; (b), (d), (f), (h): The pressure distribution along the free interface at t=0s, t=1000s, t=3000s, and t=4000s, respectively

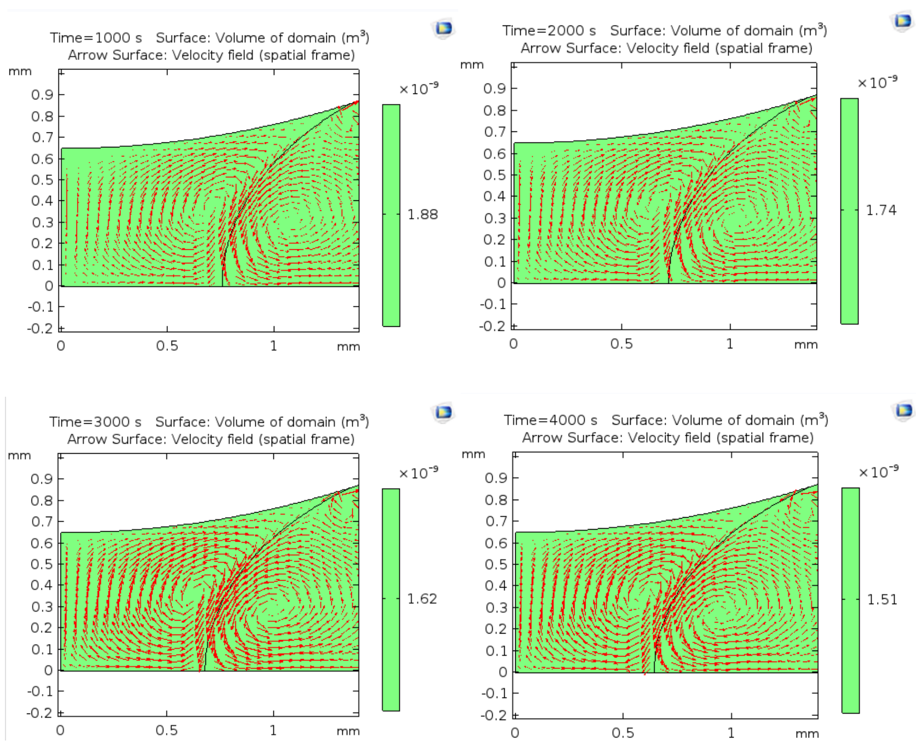

Figure 25: Flow field within the water bridge in considering the gravity

First, the gravity can influence the geometry. Figure 24 shows the influence to the pressure distribution by the gravity in the simulation. This effect is also shown in the pictures in the Appendix. The symmetry of water bridge along x axis is broken by the gravity, which causes the downward contact radius is larger than upward contact radius. Figure 25 shows the flow field within the water bridge at 1000s, 2000s, 3000s, and 4000s, respectively. The unbalance of surface tension induces the liquid near the free interface flow from three phase contact line the middle of the water bridge first along the free interface. With the change of geometry of water bridge, the flow field also changes. The liquid flows form a cell with a clockwise rotation.

Second, there should be other factors to influence the geometry such as temperature and the flow of air. The geometry of free interface is controlled by the stress balance equation. Therefore, the software bare to construct the geometry that is the connection of arc in the middle and straight line near the three-phase contact line. The similar phenomena are observed in the experimental results. The curvature of water bridge tends to be zero when it is close to the contact line. Which mean the contour of water bridge approaches to be a straight line there. However, the real situation is not as ideal as simulating situation. The temperature and the flow of air can play a role in it to influence the energy to make the water bridge be a stable geometry. The stress on the free interface cannot be balanced in realistic. The difference of geometry then appears.

Conclusions

The ALE simulations of evaporation process of water bridge between two spherical grains have been addressed via two procedures: an interface motion driven solution procedure and a vapor flux driven solution. Several components of the solutions have been formulated as follows. The effects of vapor concentration in the process zone with diffusion is established. The quantitative relationships between vapor transport and flow field are obtained. The position of liquid-gas interface is tracked according to evaporation time and volume. The flow field inside the water bridge is simulated. The gas phase flow in is obtained for the bridge exterior. The pressure distribution at the interface of the water bridge is obtained fulfilling the interface equilibrium condition. The pressure distribution simulation results are compared to the experimental results.

Most of the simulation results for the interface motion driven procedure compare well to the experimental results. However, there are substantial differences between the pressure distribution along the capillary surface obtained via interface motion method and that via flux driven method. The pressure obtained with the flux driven method do not match the experimental results.

The simulation results show that the pinning of the water bridge is imposed in the software as a fixed condition during the evaporation process. The experimental results show that the contact line obviously moves at lower separations of two grains and intermittently moves (stick and slip) at the highest separations of two grains. Therefore, the simulation process with the free interface motion yielded much more realistic results, while the pinned solution with the flux inducement is in need of substantial improvement.

The COMSOL is a powerful simulation software. However, there still are substantial limitations of its theoretical framework and numerical details as outlined by Afkhami et al [21]. The future work could improve the sub-routine of COMSOL. The behavior of water bridge should be related to other parameters, such as surface roughness, temperature, and gravity. More complicated situations should be considered, including more sophisticated theories need to be developed, including a more general framework for Laplace-Young equation.

The solution based on the interface driven procedure suggests by its agreement with experiments that the pressure, and fluid flow pattern are not strongly affected by the evaporation flux, but affected by the displacement of the interface, including that of the contact line. Finally, the evolution of flow pattern and velocity suggest that what is seen at the contact pinning may be significantly enhanced by the water flow from the bridge center toward the contact.

Appendix

The experimental data have been obtained at the University of Montpellier, Montpellier, France by Dr. B. Mielniczuk, Professors S.M. Youssoufi and Tomasz Hueckel. I greatly appreciate the possibility of using these data before their publication.

There are experimental results showing the evolution of the water bridge between two grains with 1.3mm separation during the evaporation process. The principal curvatures of the capillary surface were measured and the pressure distribution was calculated by Laplace equation (1).

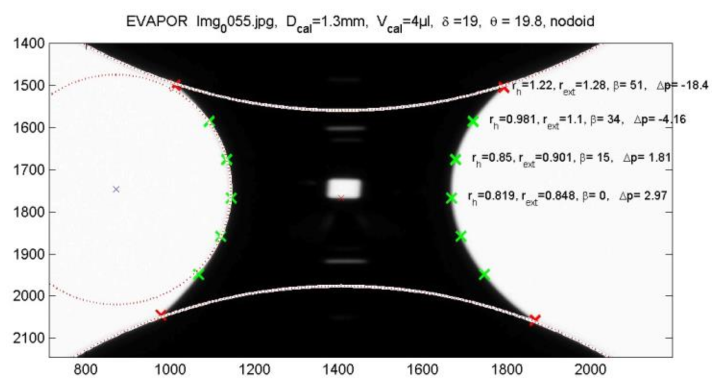

Figure 26: Geometry and pressure distribution of 1.3mm water bridge at 4µl

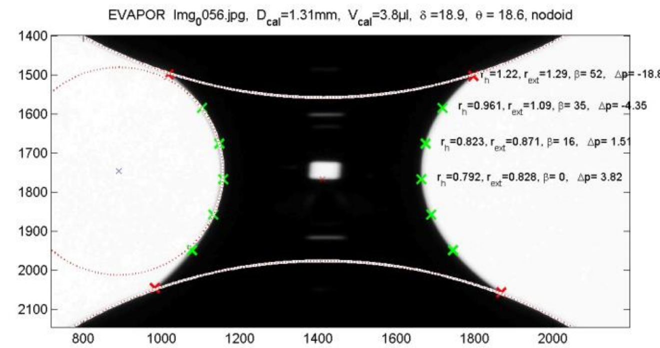

Figure 27: Geometry and pressure distribution of 1.3mm water bridge at 3.8µl

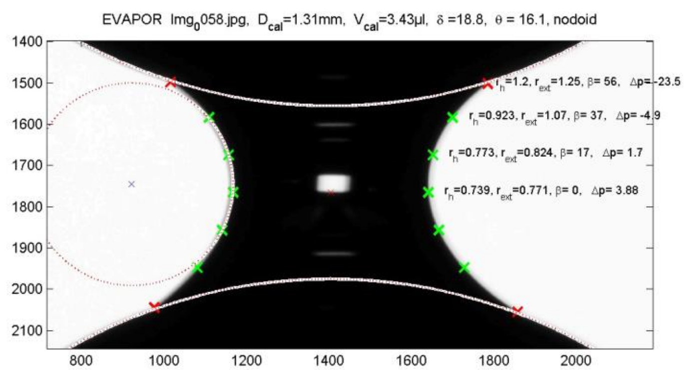

Figure 28: Geometry and pressure distribution of 1.3mm water bridge at 3.43µl

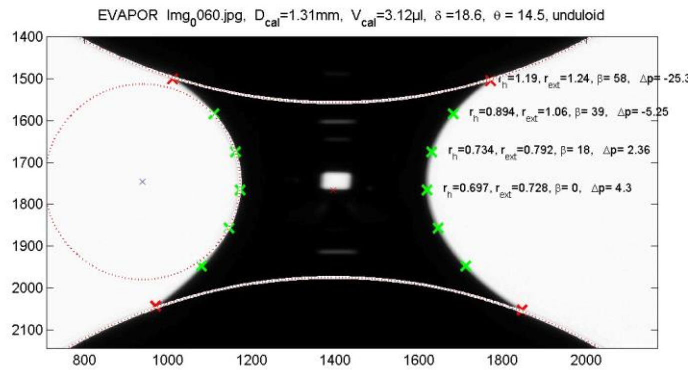

Figure 29: Geometry and pressure distribution of 1.3mm water bridge at 3.12µl

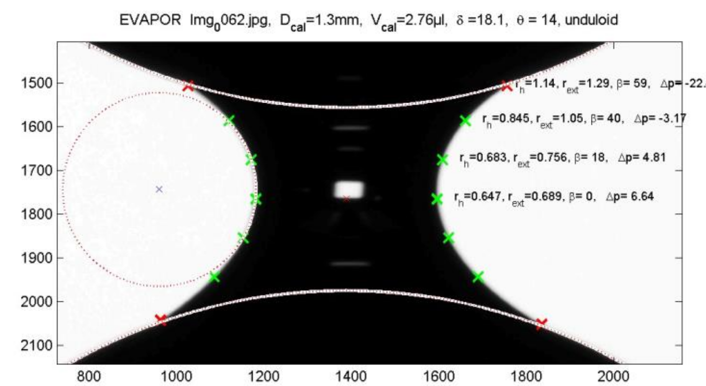

Figure 30: Geometry and pressure distribution of 1.3mm water bridge at 2.76µl

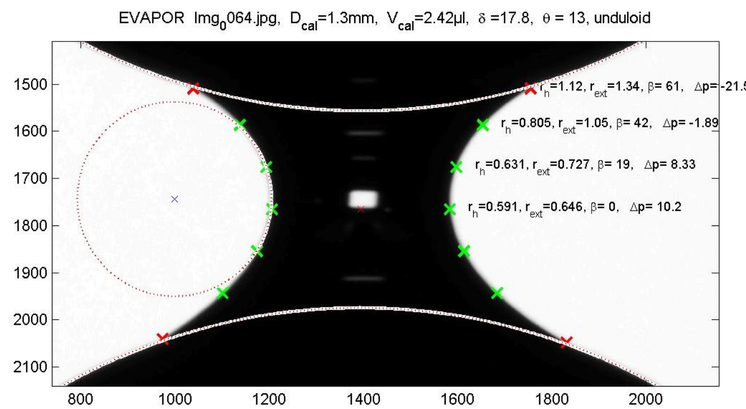

Figure 31: Geometry and pressure distribution of 1.3mm water bridge at 2.42μl

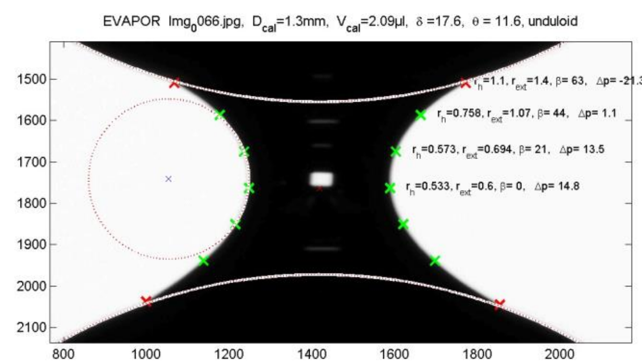

Figure 32: Geometry and pressure distribution of 1.3mm water bridge at 2.09μl

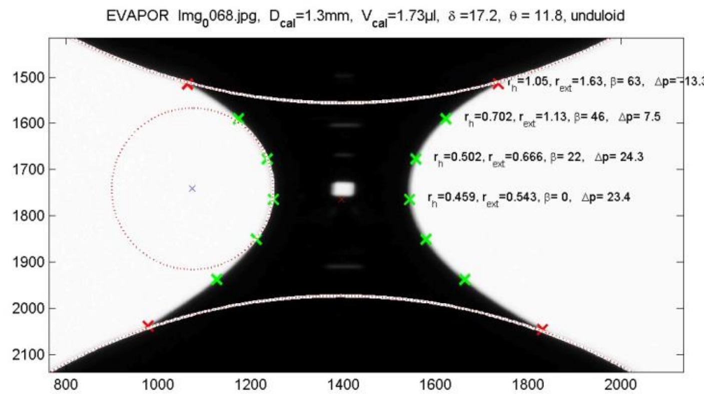

Figure 33: Geometry and pressure distribution of 1.3mm water bridge at 1.73µl

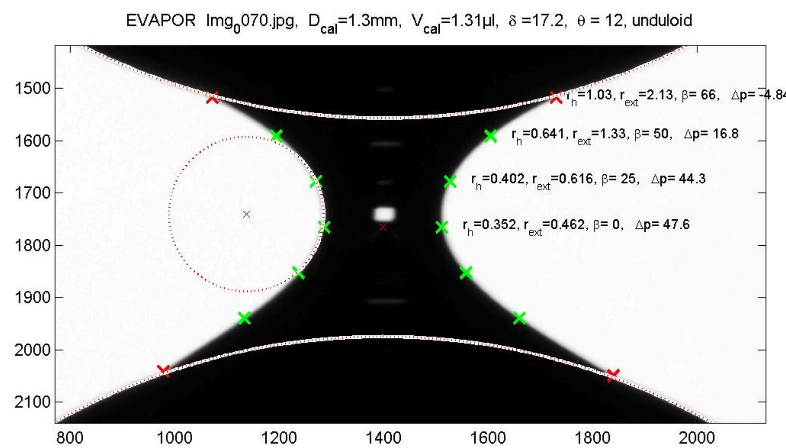

Figure 34: Geometry and pressure distribution of 1.3mm water bridge at 1.31µl

Bibliography

[1] Deegan R D, Bakajin O, Dupont T F, et al. Capillary flow as the cause of ring stains from dried liquid drops[J]. Nature, 1997, 389(6653): 827.

[2] Hu H, Larson R G. Analysis of the microfluid flow in an evaporating sessile droplet[J]. Langmuir, 2005, 21(9): 3963-3971.

[3] Brutin D, Starov V. Recent advances in droplet wetting and evaporation[J]. Chemical Society Reviews, 2018.

[4] B. Mielniczuk, O. Millet, M. S. El Youssoufi, T. Hueckel. Micro-mechanical effect of capillarity in granular media.

[5] Gagneux G, Millet O. Analytic calculation of capillary bridge properties deduced as an inverse problem from experimental data[J]. Transport in porous media, 2014, 105(1): 117-139.

[6] Deegan R D, Bakajin O, Dupont T F, et al. Contact line deposits in an evaporating drop[J]. Physical review E, 2000, 62(1): 756.

[7] Murisic N, Kondic L. On evaporation of sessile drops with moving contact lines[J]. Journal of Fluid Mechanics, 2011, 679: 219-246.

[8] Likos W J, Lu N. Hysteresis of capillary stress in unsaturated granular soil[J]. Journal of Engineering mechanics, 2004, 130(6): 646-655.

[9] Hu H, Larson R G. Evaporation of a sessile droplet on a substrate[J]. The Journal of Physical Chemistry B, 2002, 106(6): 1334-1344.

[10] Kai Yang. Simulation on hydrodynamics characteristic of sessile droplet and meniscus evaporation using arbitrary Lagrangian-Eulerian formulation.

[11] Banerjee R. Numerical investigation of evaporation of a single ethanol/iso-octane droplet[J]. Fuel, 2013, 107: 724-739.

[12] Donea J, Giuliani S, Halleux J P. An arbitrary Lagrangian-Eulerian finite element method for transient dynamic fluid-structure interactions[J]. Computer methods in applied mechanics and engineering, 1982, 33(1-3): 689-723.

[13] Liu W K, Belytschko T, Chang H. An arbitrary Lagrangian-Eulerian finite element method for path-dependent materials[J]. Computer Methods in Applied Mechanics and Engineering, 1986, 58(2): 227-245.

[14] Landau L D, Lifshitz E M. Course of theoretical physics, Volume 6: Fluid Mechanics discusses several areas of concerns regarding fluid mechanics. [M]. Elsevier, 2013.

[15] Mielniczuk B, Hueckel T, El Youssoufi M S. Laplace pressure evolution and four instabilities in evaporating two-grain liquid bridges[J]. Powder Technology, 2015, 283: 137-151.

[16] Semenov S, Starov V M, Rubio R G, et al. Instantaneous distribution of fluxes in the course of evaporation of sessile liquid droplets: computer simulations[J]. Colloids and Surfaces A: Physicochemical and Engineering Aspects, 2010, 372(1-3): 127-134.

[17] Lee K S, Cheah C Y, Copleston R J, et al. Spreading and evaporation of sessile droplets: Universal behaviour in the case of complete wetting[J]. Colloids and Surfaces A: Physicochemical and Engineering Aspects, 2008, 323(1-3): 63-72.

[18] Rowan S M, Newton M I, McHale G. Evaporation of microdroplets and the wetting of solid surfaces[J]. The Journal of Physical Chemistry, 1995, 99(35): 13268-13271.

[19] P.G. de Gennes, Wetting: statics and dynamics, Rev. Mod. Phys. 57 (1985) 827–863.

[20] E. Bormashenko, E.A. Musin, G. Whyman, M. Zinigrad, Wetting transitions and depinning of the triple line, Langmuir 28 (2012) 3460–3464.

[21] Afkhami S, Zaleski S, Bussmann M. A mesh-dependent model for applying dynamic contact angles to VOF simulations[J]. Journal of Computational Physics, 2009, 228(15): 5370-5389.